

Review of: Di Liberto et al., Lagrangian analysis of microphysical and chemical processes in the Antarctic stratosphere: a case study.

We thank the referees for the careful review of the manuscript that has allowed us to improve its content.

The new version of the manuscript now has figure 4 presenting an additional CALIOP match and figure 5 with reported the evolution of HNO₃, as detailed below. Figure 6 has now reported the O₃ range of variability observed by the balloon-borne ozonometer in the 400K ± 10K range, as red (first balloon observations) and blue (second balloon observations) areas. Figure 3 has been re-edited to enlarge the fonts. Figure 1 now present OPC data at higher spatial resolution. Below our responses to their comments, with revision of the text highlighted. We also attach a provisional version of the revised manuscript, for a broader picture of the corrections made.

Response to Interactive comments of Referee #1

(#1;1):The authors should emphasize the advances in PSC box modeling with respect to previous studies. This is the first time that I see all PSC components represented in model simulations with prescribed particle size distributions. I suggest to add an outlook on the potential of the box model with respect to the comparison to groundbased and spaceborne lidar measurements as well as regarding the understanding of PSC evolution in the polar vortex.

We have added the following lines to the end of Section 2.5 (32637,26): “Using a box model such as ZOMM for PSC studies allows a detailed microphysical calculation of cloud processes, which cannot be achieved with global models due to limited computing resources. Case studies without wind shear, as often observed in the polar vortex, offer the possibility to run ZOMM as a column version and, by doing this, to simulate also the vertical redistribution of particles. “

(#1;2):Satellite instruments: Can you please add the horizontal resolution of the MLS and MIPAS observations.

We have added the following lines to (32635,6) : “ MLS ClO profiles have a vertical resolution of 3 km in the altitude range of interest for our study, and v2.2 data are reported with a precision of 0.1 ppbv in the range 100-3 hPa. H₂O profiles have a vertical resolution of about 2-3.5 km in the range 316-0.22 hPa, a precision of 6-8 % and accuracy of 4-6%. In the region and altitude of interest, MLS horizontal resolutions in along-track direction are reported to be of the order of 200-300 km for most targets (including H₂O), 400-500 km for ClO, cross-track resolution is approx. 3 km, and the separation between adjacent retrieved profiles along the measurement track is 1.5° great circle angle (approx. 165 km). “

And to (32635,23): “ MIPAS along track sampling step is about 410 km. The width of the Field Of View at tangent point in the cross-track direction is about 30 km. The smearing of information around the tangent point given by the width of the single scan horizontal averaging kernels is 200-300 km, for most species (Raspollini et al. , 2012). However, the MIPAS products used here are

obtained by a 2-D (along track) analysis code, and its horizontal resolution is limited by the 410 km sampling step adopted in the retrievals. “

(#1;3):Trajectories: Trajectories are shown between 350 and 460 K. However, the PSC was observed between 330 and 420K. Why the difference?

The altitudes below 14 km (below approx 360 K) are only marginally impacted by the PSC, which has a very low BR there. We concentrated our attention to the more intense part of the PSC, and above that to provide a full picture of the stratospheric transport around the theta level we have then chosen for further analysis (i.e. close to the PSC top, at 400 K, where the air mass returned close to McMurdo)

(#1;4): Microphysical and optical model: page 32637, line 19-20: Can you please add studies that have used the model under those conditions.

We have revised the text indicated, as follows: “So far , ZOMM has always been initiated at typical background conditions for the winter polar stratosphere (Hoyle et al. 2013, Engel et al. 2013). The study by Engel et al. (2014) was the first study, which used the microphysical model as a column model for PSC simulations. For the present study, we developed the model further and introduced the possibility to prescribe a particle size distribution.”

(#1;5):The modeled PSC (Figure 5) only reflects the second observed layer from the lidar measurements (14 to 17km). What is the reason for that?

As reported above, we concentrated our study in the altitude region where a second passage over McMurdo occurred ten days after the first observation, i.e. close to 400 K.

(#1;6):Further, the backscatter ratio and the aerosol depolarization ratio are higher in the model compared to the lidar observations. What could be the reason for that?

Modelled Aerosol BR comes from T-matrix calculations of aerosol volume backscatter coefficient, which are done under the assumption of aspherical particles with aspect ratios of 0.9 (diameter-to-length ratio). The refractive index is 1.48 for NAT, as chosen in several earlier studies (e.g., Carslaw et al., 1998a; Luo et al.,2003a; Fueglistaler et al., 2003).

Modelled BR is around 4 at 375K (between 3 and 4 in the observations), drops to 2 at 385K (compared to 1.8 in the observations) and has a second maximum of 3 at 400K (between 2.5 and 3 in the observations,) the comparison between the modeled and observed values show a small (less than 20%) overestimation of the modeled aerosol backscatter ratio. To our knowledge, the order of magnitude of such mismatches is what is to be expected when performing optical computations on observed particle size distribution (see, as instance, Cairo et al., 2011). For what concerns the aerosol depolarization , the modeled depolarization stays at values between 0.4 -0.6 throughout all the PSC history, thus demonstrating the NAT nature of the PSC cloud during its lifetime. In the initial stage of the modeling, its value hovers around 0.6 throughout the PSC extension, which is 30% higher than the observed values of 0.40-0.45. The discrepancy between the modeled and observed depolarization may stem from the assumptions on particle shape and aspect ratio: as instance, T-matrix simulations (Liu et al., 2001) show that aerosol depolarization may vary as much as 50% depending on the aspect ratio and shape of the modeled particle. Increasing asphericity

would result in lower values of aerosol depolarization. However, the arbitrariness in the choice of such parameters in the optical computations does not hamper the main finding of the model exercise, that the cloud remained of NAT type throughout its lifetime. Moreover, the choice made of average values of aspect ratio and shapes, assures that the particle area density is not significantly affected by their uncertainty.

(#1;7):The bimodal lognormal distribution is only fitted to the PSC observation between 14.5 and 16 km. Why not over the entire altitude region of the observed second PSC layer between 14 and 17 km?

In fact, the usual processing of OPC data provides mono and/or bimodal fittings wherever particles are present and counted with sufficient statistics. In the sentence reported in our paper, we meant that in the region between 14.5 and 15 km (15, not 16! This typo has now been corrected in the revised version of the manuscript) this processing produced an average estimate of 22 ppb HNO₃ in condensed phase. Please see also our response to (#3;1).

(#1;8):Chemical simulations: results are only shown for 400 K. However, the double overpass of the air-mass was between 380 and 420 K. Are the simulations robust for the entire altitude region?

The model simulations represent the altitude region 380-420 K in a qualitative way (they correspond to an “intermediate“ situation), but not in a strict quantitative way. To be more specific, if the initial ClO_x concentration varied monotonously with altitude, we might conclude that the amount of O₃ depletion, attributable to the ClO_x present at the beginning of the trajectory, at 400 K, is “intermediate” between that at 380 K and 420 K. However we do not have ClO_x with a sufficient vertical resolution to check whether ClO_x really varies monotonously with altitude. In fact, a similar statement on monotonicity is not true for the O₃ mixing ratio: it has a minimum near 400K and is larger at both 380K and 420 K. Moreover and more important, for what concerns the effects of heterogeneous chemistry along the trajectory, it must be stressed that the comparison of runs with and without heterogeneous chemistry depends critically on the PSC present along the corresponding trajectory. As we investigate an altitude at the upper edge of the PSC, a change in altitude significantly changes the PSCs along the trajectory (higher altitude: less or even no PSC; lower altitude: more PSC). Thus the results at a different single altitude may differ from those at 400K.

(#1;9):Figure 5, upper panel: altitude axis is partially covered.

Figure 5 has been re-edited.

Response to Interactive comments of Referee #2

(#2;1):On p32643 l23 the authors note that limb measurements average over large horizontal distances which makes analyzing processes in small portions of air difficult. This also applies to the initialization of the trajectories. It might be helpful to look at daily maps of MLS or CTMs to assess the homogeneity of the vortex in the vicinity of the trajectory initialization. Especially, the uncertainty in ClO_x is of interest in modeling ozone loss. Quantifying the uncertainty here will add value to the authors calculation of ozone loss.

We have added the following lines to (32638,11) “ inspection of MLS maps for H₂O, HNO₃, ClO, O₃, HCl, N₂O available at 56 hPa level at http://mls.jpl.nasa.gov/plots/mls/mls_plot_locator.php for 10 September 2010, shows relatively low meridional gradients of the species of interest over McMurdo, thus giving confidence on the low spatial variability of the values used to initialize our model calculations. “

For what regards the impact of the ClO uncertainty, please refer to our answer to (#2,9)

(#2;2): In this context, please add the in-situ measured ozone mixing ratios to Figures 6 and 8.

Done.

(#2;3): From Figure 2 it appears that on 20 September ozone at 400K is at about 100 ppbv. Is the calculated ozone loss along the trajectory in agreement with this?

Figure 2 shows at 400K that ozone changes from 400 ppbv to 100 ppbv in 10 days, which provides an ozone loss of approx. 30 ppbv/day. This estimation, which remains fairly constant in a 5K range from the 400K level, is in fair agreement with the modeled ozone loss of 35 ppbv/day reported in the Conclusions paragraph (line (32647,23)).

(#2;4): Please discuss how good the model reproduces the observed ozone loss.

The remark outlined in answer to (#2,3) above has been introduced in the text. We have added to (32647,23) the following lines.

“...35 ppb day⁻¹, in fair agreement with an ozone loss of approx. 30 ppbv/day that can be deduced from the balloon data. We should note that the value of the modeled ozone loss rate is within the ranges reported in the literature (Schofield et al., 2015) and the difference between its value whether heterogeneous chemistry on PSC particles has been considered, or not, is beyond both its reported atmospheric variability, and the sensitivity of our measurements.”

(#2;5): The authors have observations of all relevant species and can add value to the discussion concerning the parameters determining the ratio of ClO/Cl₂O₂. Are the recommended values for the Cl₂O₂ recombination constant and photolysis frequency in agreement with ozone loss observations (for details see von Hobe et al. (2007), doi: 10.5194/acp-7-3055-2007)?

The model simulations, using reaction rate constants from JPL 2011 (including the Cl₂O₂ recombination constant $K_{\text{ClO}+\text{ClO}}$ and Cl₂O₂ photolysis frequency $J_{\text{Cl}_2\text{O}_2}$), are consistent with the O₃ loss observed (see Fig. 6a). However, the information that we have is not sufficient to draw conclusions about individual reaction rate constants: We know two numbers that are relevant for the O₃ loss by the Cl₂O₂ cycle: the ClO mixing ratio at (near) the beginning of the trajectory and the O₃ loss along the trajectory. In an ideal case (no errors at all) it would be possible to draw conclusions on two “unknown” numbers, e.g. $K_{\text{ClO}+\text{ClO}}$ and a scaling factor for $J_{\text{Cl}_2\text{O}_2}$. However, the errors associated with the observations (measurement errors, spatial averaging by satellite sensors, distance between the measurement and the corresponding trajectory point) are much too large to allow such an inversion. Significantly more data and the application of statistical methods would be needed.

(#2;6):The authors should discuss the uncertainty of their trajectories. From Figure 3 it appears that after 10 days trajectories which had been started around the same altitude (400K, cyan) spread some hundred kilometers. The authors could start several trajectories around the initial balloon profile and monitor their spread after ten days.

A trajectory cluster analysis has been performed, using NCEP/NCAR reanalysis. Isentropic forward trajectories have been launched, each member of the trajectory ensemble calculated by offsetting the starting lat-lon position by 1° and the vertical position by 400 m upward and downward (corresponding approx. to 5 K). The trajectory cluster remained geographically confined, passing over the McMurdo longitude with a latitudinal spread of approx. plus or minus 5°, roughly centered over McMurdo. The overpassing occurred on average after 9.5 days, with a time spread of approx. 0.5 days. We have further tested the dependency on the particular trajectory model by using three different trajectory models, computed from meteorological fields from different analysis centers: Goddard Space Flight Center (gsfc), NOAA (Hysplit) and European Centre for Medium-Range Weather Forecasts (ECMWF) using the ERA Interim meteorological database. The differences between the three different models of trajectories are very small and mainly due to different airmass speeds .

(#2;7):Is the 400K isentropes representative for the 380-420K range where the air mass returned over McMurdo after 10 days? From Figure 5 it appears that 400K is at the upper edge of the PSC and the authors note on p32645 19 that sedimentation prevents NAT particle existence after two days. At 380K NAT appears to be present until the PSC evaporates, how does this influence heterogeneous chemistry?

As noted by the reviewer, the 400K isentropes is peculiar in the sense that it is at the upper edge of the PSC, hence is the region where sedimentation is more likely to produce an effect on heterogeneous chemistry, as the particles removed are not replaced by particles settling down from above. This is why the models were run at 400K only. The modeled study on the effect of sedimentation has been carried out by running twice the chemistry model at 400K, fed with particle surface areas coming from the PSC microphysical model both with and without sedimentation taken into account. We believe this approach is more effective than studying the evolution at 380K.

(#2;8):Add information about H₂O and ClO MLS products to the discussion.

Please refer to answer to remark (#1;2)

(#2;9): MLS v2.2 has a known bias in ClO (Santee et al. (2008), doi:10.1029/2007JD008762), has this been accounted for in the initialization?

The initialization is based on a ClO amount derived from v2.2 MLS data. At the time of writing the manuscript, we did not take into account the bias present in ClO, studied in detail by Santee et al. (2008). In their work, they assessed a substantial (~0.1–0.4 ppbv) negative bias that may be present in the v2.2 ClO values at retrieval levels below (i.e., pressures larger than) 22 hPa.

The ClO product has been significantly improved in v3.3; in particular, it is reported (Livesey et al., 2013) that such negative bias has been largely mitigated, primarily through retrieval of CH₃Cl (a new MLS product in v3.3). In particular, it is reported that virtually no bias remains at 32 and 46 hPa, and only small biases may still be found at 68 hPa. We checked that the difference between the

initial ClO values derived from v2.2 and v3.3 are not higher than 10% for that particular day, location and pressure levels (68 and 46 hPa we used to interpolate the value at 400K, see answer to (#2,10)). Same results of the v2.2 and v3.3 comparison are found for some other profiles chosen at random around 10 September 2008, finding differences below 10%.

We performed a sensitivity analysis assuming that ClO and Cl₂O₂ were in chemical equilibrium at the time of the measurement (ClO+ClO+M->Cl₂O₂+M, Cl₂O₂+hν->ClO+ClO), and increasing the initial amount of ClOx taking into account a negative bias of 10% of the MLS value with respect to the true value. Such increase of initial ClO would have some visible consequence for the O₃ loss, after 8 days of model running, as depicted in figure A1.

We estimated that such bias would not produce qualitatively significant consequences (a 10% of available ClO would produce an additional 2.5 ppbv/day), and we decided to keep the initial value of ClO as derived from v2.2.

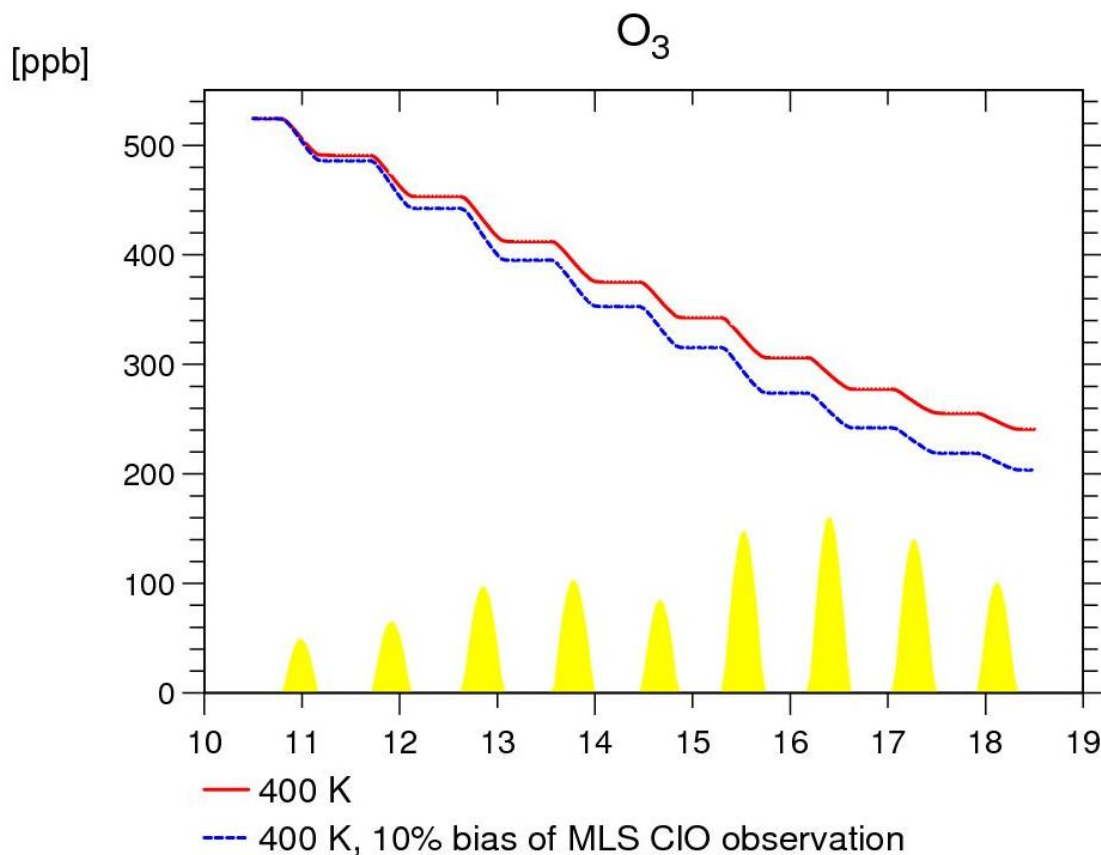


Figure A1: Red line, evolution of O₃ with the amount of ClO prescribed according to MLS values. Blue line, evolution of O₃ with a 10% increase on initial ClO values. The model was run with heterogeneous chemistry and sedimentation taken into account.

(#2;10): Also, has the MLS averaging kernel been taken into consideration?

We do acknowledge the fact that, due to a relatively coarse vertical resolution, satellite data we use to initialize model runs at a given altitude, or compare with the model results, do not correspond exactly to a given altitude, but represent a weighted average of mixing ratios at different altitudes

(which may be expressed by the averaging kernel). However, we think this is the best we can do, because a correction or an elimination of the effect of the coarse resolution of these data is not possible.

If the referee comment has to be intended in the sense that, to compare model results to MLS data, we should process our results with the MLS averaging kernel in order to avoid the presence of fine structures in our results which cannot be resolved by MLS, then the answer would be that we do not see any reason for doing this in our study since we compare to MLS, only results from one single trajectory. To use the averaging kernel, we should have worked with many trajectories at different altitudes.

A final note is due to explain how we have used the MLS, available on pressure levels, in our simulation on a constant theta level. We have interpolated the MLS data x_1 and x_2 , available from the web database at pressure level P_1 and P_2 , to retrieve the data x at the pressure level p corresponding to the 400K theta level, by means of the following formula:

$$(\ln P - \ln P_1) / (\ln P_2 - \ln P_1) = (x - x_1) / (x_2 - x_1)$$

A similar approach is suggested in Ridolfi et al. (2010). Correspondence between pressure P and the 400 K theta level were retrieved from the pressure and temperature data of the 10 September McMurdo balloon sounding.

(#2;11): Add a Figure comparing ZOMM results (backscatter and depolarization) to intersecting CALIPSO overpasses (red circles in Figure 4). How does ZOMM perform in reproducing the PSC several days after the initialization?

We broadened our CALIOP match criteria and considered CALIOP profiles during night time and matching the $\pm 1.0^\circ$ latitude, $\pm 2.5^\circ$ longitude, ± 12 h time difference criteria, with respect to the traced air mass location. By doing this, we were able to add another reasonable comparison on 11 September 2008. ZOMM backscatter results seems to overestimate the CALIOP profiles as seen in Fig. A2. This might be for the relatively large matching criteria, or for the same reason as we do overestimate the condensed HNO_3 as described in (#3;1). However, the simulated location and altitude range of the PSC is in good agreement with the observations.

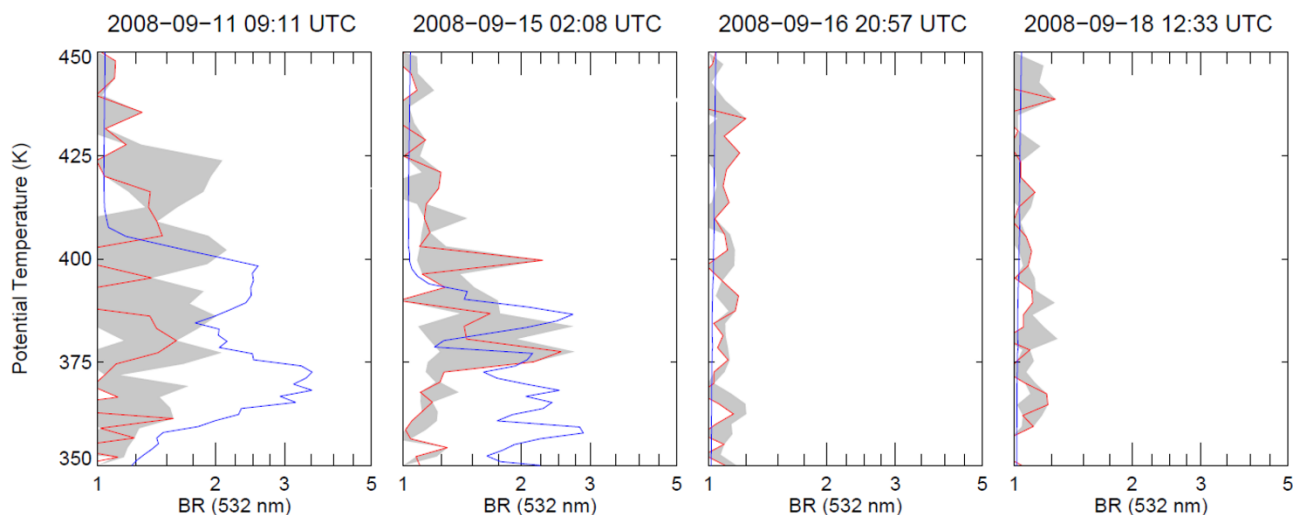


Figure A2. Comparison between ZOMM and CALIOP. Simulated ZOMM backscatter ratios are shown in blue calculated for 532 nm. The gray shaded area comprises maximum and minimum backscatter values from CALIOP within a range of +/- 50 km around the CALIOP profile in red, which is closest to the 400 K trajectory.

Figure 3 in the manuscript was updated to include the 11 September 2008 match, and the text revised accordingly.

(#2;12): How does sedimentation of NAT particles change the abundance of HNO₃ within the PSC? Please add a panel showing total HNO₃ to Figure 5 so the layers of denitrification and re-nitrification become visible. The vertical extent of the PSC alone is rather inaccurate to quantify the extent of particle sedimentation and evaporation.

The following panel (Figure A3) , has been added to fig. 5 in the manuscript, as requested.

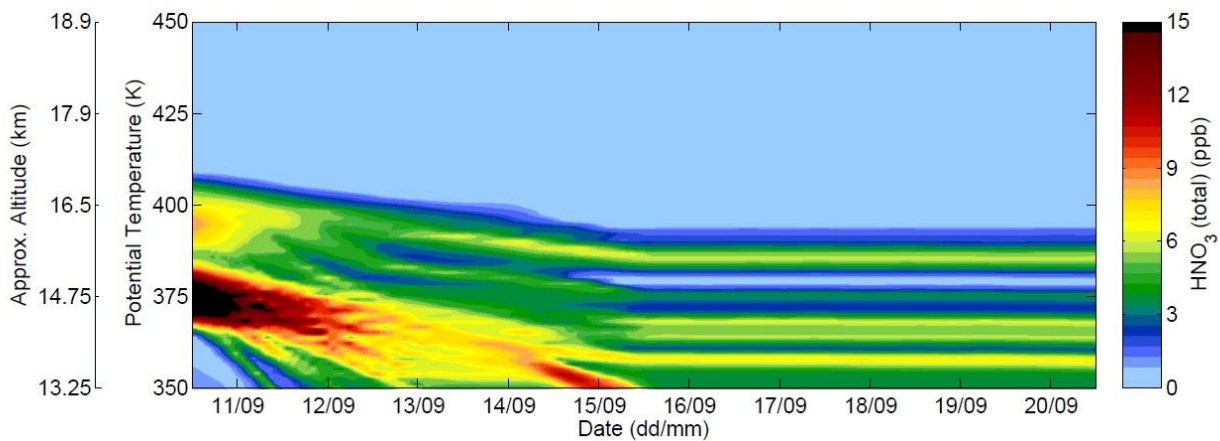


Figure A3: Evolution of total HNO₃.

MLS data do provide evidence of a large vertical redistribution of the HNO₃ in the gas phase after the evaporation of the PSC.

Figure A4 shows MLS HNO₃ profiles taken at the geographical location of the 400K trajectory, on September 10 and on September 15 along the 400K. Even taking into account the coarse vertical resolution of the data, a descent of the HNO₃ peak can be clearly discerned. The order of magnitude of the HNO₃ amount matches with the results of the simulation.

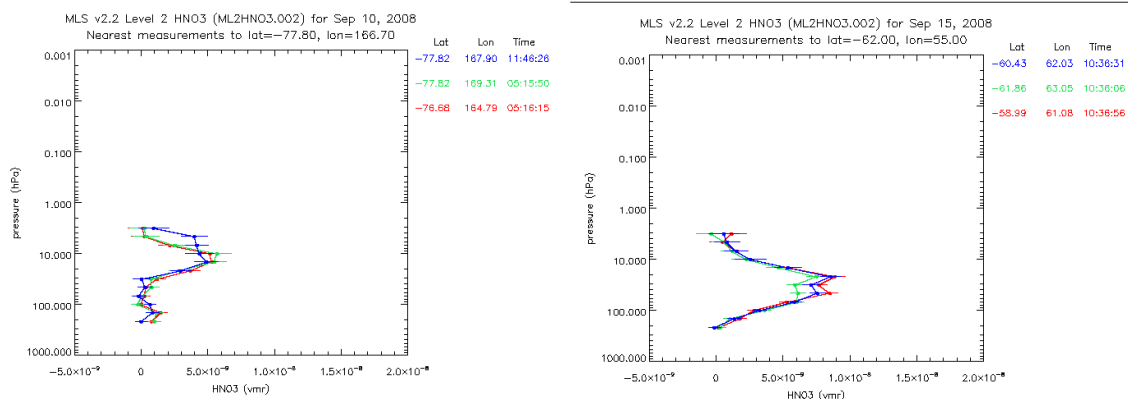


Figure A4: MLS profiles on 10 September (left panel) and 15 September (right panel), at locations where the 400K airmass was.

(32642,3) and following have been modified as: “Figure 5 shows the modelled evolution of the PSC in terms of Backscatter Ratio (upper panel), Aerosol Depolarization (middle panel) and total HNO₃ (lower panel) during the 10-20 September period.

The persistence of the PSC for almost a week is evident. The cloud remains of NAT type for 6 days after the first McMurdo balloon sounding, and totally evaporates three days before the second McMurdo sounding, as a warming caused its disappearance before 16 September. This warming in the second part of the trajectory coincides with an increasing distance of the airmass from the vortex centre. A vertical redistribution of the cloud is also evident, caused by the modelled particle sedimentation. The cloud vertical extent changes from 410-360 K (approx. 17-14 km in geometrical altitude) to 390-350 K (approx. 16.5-13.5 km) in 6 days. A large vertical redistribution of the gas phase HNO₃ can be seen after the evaporation of the PSC. This occurrence has been confirmed by MLS HNO₃ data on locations along the 400K trajectory.”

(#2;13): So far it has only been shown that ZOMM agrees with observations that after 10 days the PSC has evaporated. To conclude that the evolution and type have been reproduced an intermediate comparison with CALIPSO should be shown.

Please refer to what written in response to question (#2,11)

(#2;14): How does the modeled ozone depletion rate compare to the measured O₃ change between both sondes and how does this rate compare to previous studies like MATCH campaigns?

As quoted in response to question (#2;3), figure 2 shows at 400K that ozone changes from 400 ppbv to 100 ppbv in 10 days, which provides an ozone loss of approx. 30 ppbv/day. This estimate remains fairly constant in a plus/minus 5K range from the 400K level, and is in fair agreement with the modeled ozone loss of 35 ppbv/day reported in the Conclusions paragraph (line (32647,23)).

In contrast to the Arctic (von der Gathen et al., 1995; Rex et al., 1998, 2002), Antarctic ozone loss rates by means of Match campaigns have been relatively less studied. A recent article producing loss rates from ozone observed in situ over long periods of time by specially designed ultraviolet photometers flown on long-duration balloons launched in the first half of September 2010 as part of the Concordiasi campaign (Rabier et al., 2013) out of McMurdo Station (Schofield et al., 2015) reports a vortex average ozone loss rate of 74 +/-70 ppbv/day over the 410-430 K range, our values are within such variability. The Schofield et al. (2015) reference has now been cited in the text (see our answer to comment (#2;4)).

(#2;15): Figure 6: Describe how the error bars on the satellite observations were determined

Errors bars associated to MIPAS satellite data are the retrieval errors due to measurement noise on the used single values. For MLS data they are derived from the precision reported in the data files (see for description Livesey N. J., 2011) propagated to the 400 K interpolation level (see our answer to (#2,10),

Response to Interactive comments of Referee #3

(#3;1): My major concerns is the estimate of condensed nitric acid... ...the result would be more convincing if appropriate values of condensed NAT were used.

The sentence in (32641,25), which has raised the perplexity of the referee, is incorrectly expressed. In fact the number reported there refers to values encountered between 14.5 and 15 km. In the microphysical simulation at 400K, which we analyzed in further detail afterward, the initial value of total HNO₃ is around 7 ppb, and the gas phase HNO₃ is 1.7 ppb. In fig. A5, the evolution of total (left) and gas phase (right) HNO₃ at 400K is shown, for the case when denitrification is acting (red line) or not (blue line).

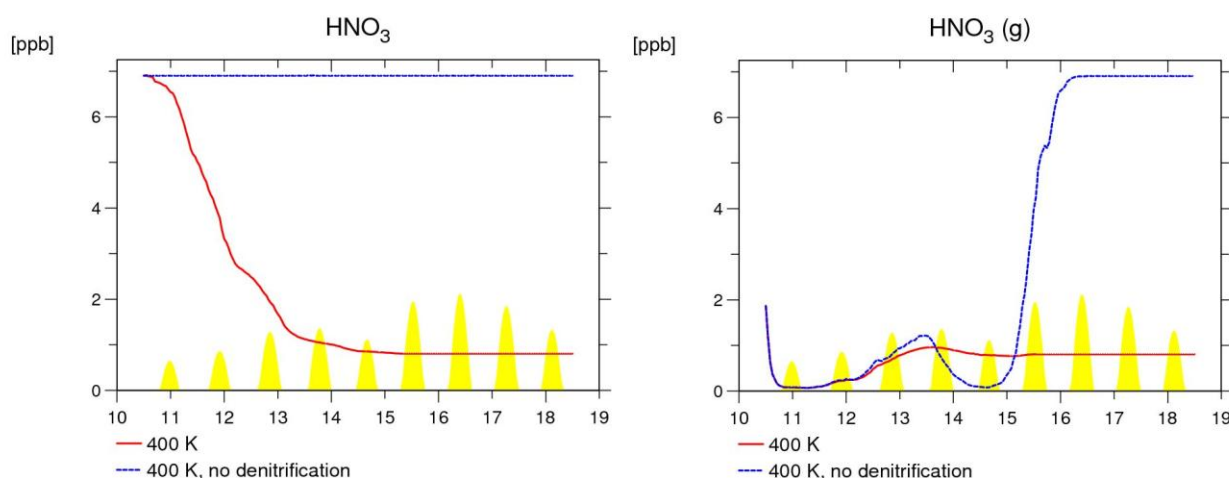


Fig. A5: Total (left) and gas phase (right) HNO₃ evolution at 400 K, from the microphysical model with (red line) or without (blue line) sedimentation

Much higher values of total HNO₃ were reached close to 370 K, where such enrichment can probably partly be due to sedimentation, occurred in the previous days. However, as suggested in the revised text, the value of 22 ppbv HNO₃ in the NAT particles, met in some region of the cloud, computed assuming spherical particles in the largest lognormal mode, may be an overestimation, based on the HNO₃ expected to be available, but not based on the particle measurements. The particle measurements were looked at closely and there seems to be no reason to dismiss the estimates of particle volume from them. The large particle concentrations are significant (0.1 cm⁻³) and the particles are large 2-4 μm. Thus the measurement uncertainties are not large. Both lognormal fits and simple histogram summations lead to similar estimates of particle volume, which, given the assumptions above lead to the large estimates of condensed HNO₃. The paper of Molleker et al. (2013) confronts a similar problem, reporting Arctic HNO₃ mixing ratio in condensed phase up to 17 ppbv ±40 % (observations on January 2010) and up to 25–35 ppbv ±40 % (11 December 2011), derived from a particle diameter estimation based on the hypothesis of spherical particles combined with an assumption of a pure NAT composition. Although large HNO₃ containing particles were consistently observed by a condensed phase NO_y instrument operated at the same time of the optical particle counter, nevertheless in general the particle volumes seemed to overestimate the HNO₃ content in the condensed phase. Two possible explanations were put forward, namely (i) non-compact or non-spherical NAT particles, and/or (ii) NAT coating on

preexisting ice particles. In our case, hypothesis (ii) cannot be ruled out due to the previous thermal history of the air mass at 400K which would have allowed ice formation in the week before our observation. We must acknowledge the fact that NAT particles may have larger apparent sizes compared to compact spherical particles, e.g. due to non-compact morphology or aspheric shape or ice presence. In any case, either NAT coated, or high aspect ratio, or spongy particles, would lead to a reduction of our estimation of condensed HNO_3 that would be basically unpredictable, leaving us with only the resource of educated guesses, as the one (4-5 ppbv in condensed phase) correctly suggested by the referee. It is worth noting that all these hypotheses put forward to reconcile particle dimension with HNO_3 content, would impact particle settling speeds as well, but unfortunately in opposite directions, again leaving us in uncertainty. That is why we decided to stay with the assumption of compact, spherical NAT particles but acknowledge here the fact that our assumption leads to HNO_3 in condensed phase which may be an upper limit (we delete the sentence “considered realistic” in (32641,26) and to discuss what may be the consequences of reducing the condensed HNO_3 , in our results.

Lines (32641,18) –(32641,26) are rewritten as:

“With these assumptions estimates of HNO_3 content in the particles larger than $\sim 0.3 \mu\text{m}$ ranged from 20-30 ppbv from 370-385 K (14.5-15.5 km), to near 10 ppbv from 385 – 405 K (15.5-16.8 km). While these values are higher than expected, they result from the OPC measurements of significant concentrations ($\sim 0.1 \text{ cm}^{-3}$) of particles in the 2-3 μm range, so are not easily dismissed. A possible overestimation of the HNO_3 content in the condensed phase from particle size measurements was reported in some recent airborne measurements from the RECONCILE campaign (von Hobe et al., 2013) and possible reasons for that are extensively discussed in Molleker et al. (2014). The microphysical run was initialized with an estimate of the initial value of total HNO_3 of 6.9 ppb, of which 5.2 ppb in condensed phase, considered as a realistic upper limit for the amount of HNO_3 in the particles. “

(#3;2): On what scales do you expect these processes to occur and how will this smearing effect impact your analyses?

The problem of smearing out temperatures and winds from meteorological analysis, and trace gas concentrations from satellite fields, is present and unavoidable every time box models are used in process studies and compared with those datasets. In our work, subgrid temperature fluctuations are superimposed to synoptic scale temperature histories for the microphysical simulations. For what concerns small scale fluctuations in trace gas fields, they exist as documented in many stratospheric aircraft in situ measurements. As instance the recent Rolf et al., (2015) paper shows 50% ozone fluctuations over linear distances of few hundreds of km, in Antarctica at 16 km altitude (flight on 13 September 2012). Inspecting the data set in our possession indicates that satellite trace gases maps do not show strong and large gradients over McMurdo during the time of our in situ observations, and that the Eulerian observation of the large PSC event over McMurdo during 10 September 2008 show a significant stability of the cloud in terms of optical properties and spatial distribution during the course of the balloon measurements. This information has been introduced in the revised text.

(#3;3): Why haven't you compared the CALIPSO data with the model calculations in a more quantitative fashion?

Please refer to our answer to (#2;11)

(#3;4): P.1, L.27-29: M L.27-29: Minor point- the use of 'conversely' here seems inappropriate.

This has now been deleted.

(#3;5): P.2, L.58: You state here that Antarctic PSCs are predominantly type NAT? (...) Are your 'type NAT' PSCs actually liquid/NAT mixture PSCs.

We reformulated the sentence in (32631,16-17) as follow: "STS-NAT mixtures are the predominant composition classes of PSC observed throughout the stratosphere from mid-June until mid-September in Antarctica, with NAT particles prevailing at altitudes above 15 km. (Pitts et al., 2009). Over McMurdo, PSC of prevalently NAT type appear in early June..."

(#3;6): P.3, Section 2.3: You don't mention the horizontal resolution (cross-track and alongtrack) of the MLS or MIPAS instruments, which can be hundreds of kilometers. I think this information is relevant to the study and should be mentioned here.

Please refer to answer to remark (#1;2)

(#3;7): P.3, Section 2.3: The coincidence criteria for MLS and MIPAS is about +/- 200 km and for CALIPSO is about +/- 100 km. Given the spatial variability of the gas species, PSCs, etc., how do changing these criteria impact the comparisons?

We have tried larger criteria for the gas phase, but doubling the acceptance radius increases the number of coincidences with the only benefit to add more scattered point. For what concerns the gas phase, 200 km seemed a good compromise between data statistics, average length of gas phase gradients and the distance from McMurdo of the air mass sampled the second time. PSC spatial variability can occur on much smaller spatial scales, so we had chosen to narrow CALIOP coincidence criteria. However, in the revised version of the manuscript, the coincidence criteria for CALIOP have been widened to match the MLS and MIPAS, the text of the revised manuscript has changed accordingly (please refer to our answer to (#2,11)).

(#3;8): P.3, L.232: CALIPSO and Aura are in the same orbit, but Aura was repositioned in early 2008 and now CALIPSO and MLS make measurements within about 30 s of one another. MLS profiles are separated by about 165 km along the orbit, while CALIPSO samples on a much finer horizontal resolution of ~1 km in the lower stratosphere. See Lambert et al., Atmos. Chem. Phys., 12, 2899–2931, 2012 for more details.

This information, and the suggested reference, has been inserted in the text:

(32636,9-11) "The CALIPSO and Aura satellites are part of the A-train track (Stephens et al., 2002). Since early 2008 CALIOP and MLS make measurements within about 30 s of one another. MLS profiles are separated by about 165 km along the orbit, while CALIPSO samples on a much finer horizontal resolution of approx. 1 km in the lower stratosphere (Lambert et al., 2012)."

(#3;9):P.4, Section 2.5: I'm somewhat familiar with the standard ZOMM, but not the column version. Can you describe in a little more detail how sedimentation is handled? Does it assume that the entire column of air is moving at the same velocity and in the same direction (i.e. no horizontal or vertical shear)? Are these reasonable assumptions in this case? I could imagine near the vortex edge this would not be the case. How do these assumptions potentially impact the results?

The approach of using a column model is indeed only possible in situations without horizontal wind strain or vertical wind shear. Changes in wind direction or velocity with changing altitude would otherwise lead to errors in the location of the sedimentation events. However, at 400 K, the trajectories stayed sufficiently close to meeting the criteria of a homogeneous wind field. In the figure A4, hereby reported, a quality criteria was introduced to check whether the trajectories were diverging. The presented horizontal displacement is calculated over a vertical distance of 500 m. As can be discerned from the figure, the assumption of a homogeneous wind field was reasonably good throughout the lifetime of the PSC, at the altitudes of interest. After 15 September and below 350 K, the assumption of a homogeneous wind field is not fulfilled.

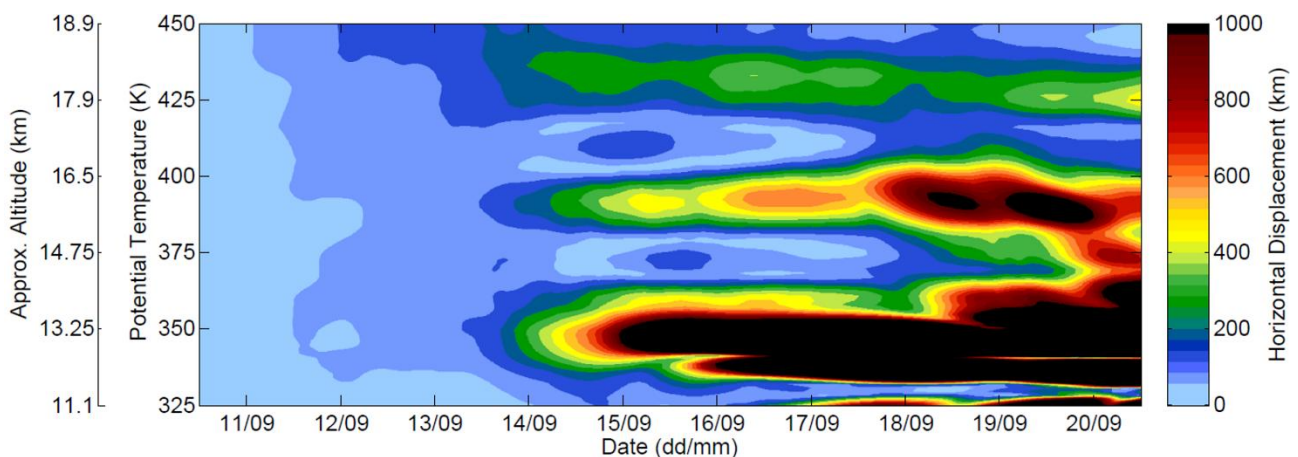


Figure A6: Horizontal displacement between air mass trajectories originating from McMurdo and run 10 days forward. The horizontal displacement is calculated considering an altitude range of 500 m.

(#3;10):P.4, L. 303-305: Are these MLS measurements assumed to be representative of the total (gas phase + condensed phase) abundance? How is uptake on PSCs estimated?

MLS measurements presented here are concerned with gas phase only.

(#3;11):Can the coarse resolution of MLS accurately capture the scales of the processes of interest?

Probably not if PSC occurs in highly localized regions whose spatial extensions is smaller than the horizontal resolution of the limb sounder, as PSC processing of air may create gradients of species within the spatial resolution of the sensors. However, as instance, Santee et al. (2002) studied the redistribution of HNO_3 in the Arctic due to PSC particle sedimentation by following the PSC evolution from formation through dissipation with a Lagrangian approach, and concluded that every time the models displayed large changes in either HNO_3 or aerosol extinction, they were reflected in the MLS data.

In our study, of course, there can be a degree of inaccuracy of the trace species observed by the satellite, due to their inherent spatial average, and we indicated that in the text as a possible explanation for the coarse comparison between model results and data, The extent of this inaccuracy cannot be known a priori.

(#3;12):P.4, L. 325-326: How far did the balloon fly downwind from McMurdo during the four hour flight? How much variability was there in the lidar measurements over the four hour period? This would provide some insight into how homogeneous the PSC field .

The PSC observation occurred in approx. 70 minutes out of the 4 hour balloon flight duration, and the balloon flew approximately 50 km. During that time window, the optical parameters of the PSC observed by the lidar over McMurdo remained quite stable and consistent. This information has now been added in the text:

(32638,24-32639,2) “A PSC was observed for 70 minutes in the initial part of the flight, during ascent, over a horizontal distance of approx. 50 km. The left panel of Fig. 1 depicts the lidar backscatter (solid line) and aerosol depolarization (dotted line) ratios vs. altitude, averaged over the OPC observation time, while the right panel shows the particle size distribution measurements obtained by the OPC.”

(#3;13):P.4, L.335-340: Is it likely that there were also STS droplets present in this ‘NAT’ cloud? What number concentration of STS is present?

As reported in (32642,15-16), we have assumed that the smallest size bins of the measured size distribution (particles < 0.3 μm radius) consisted of liquid STS droplets. Their number concentrations can be discerned by inspection of Figure 1.

(#3;14):P.4., L.358: Same comment as earlier- do you think 300 km is sufficiently close for an overpass to assume the balloon and lidar are sampling the matched air mass?

The study has been done under that assumption. 300 km is a value that lies at the lower range of variability of match radii used in previous studies.

(#3;15):P.5, L.367-370: Can you speculate on what caused the very different ozone values in the uppermost part of the soundings? Is this a chemical or dynamical effect? Does this imply that the air in the column may be exposed to horizontal or vertical shear and therefore the ZOMM column model would not be representative?

The air sampled on 20 September 2008, in the uppermost part of the sounding, had a different origin with respect to the 390-410K layer. On 10 September, this latter layer was above McMurdo, while the former was displaced more than a thousand km northward. Moreover, from 10 Sept onward, the air above 410K never experienced temperatures low enough to allow PSC formation. As the two soundings sampled different airmasses, on the 10 and 20 September, we could not speculate about ozone loss rates based on such observations as they are certainly to be ascribed to both chemical and dynamical effects.

We do not share the view that, since the air in the column over McMurdo on 10 September was exposed to different horizontal winds, therefore the ZOMM sedimentation could not be used. We

concentrated our study on the top part of the PSC observed on 10 September. There, sedimentation acted to remove particles from that level, but not to deliver additional particles settling from above, as there was no PSC above. Therefore at that particular level the possible wind shear do not impact the microphysical model results and how they have been used in the chemistry simulation.

(#3;16):P.5, L.376-378: Are these ozone losses observed in the past also representative of the ten-day time scale of this study?

The time scale of our study is of the same order as those considered in previous Match campaigns. Please refer also to response to comment (#2;14) for a comparison between ozone loss rates.

(#3;17):P.5, L.400: Why are there not more MLS values coincident with CALIPSO in Fig. 3? Am I misinterpreting the figure?

We used all MLS data available on its database, which we acknowledge are in fact less than MLS passages over the trajectory. The reason for this lack of data in the database is unknown to us.

(#3;18):P.5, L.404-422: It seems like you could find good coincidences with CALIPSO on almost every day-or at least find a representative CALIPSO orbit. Are there CALIPSO orbits available on 10-15 September, but not shown? The CALIPSO data as currently used does not add much to the paper- other than show that there was a PSC in the area.

Please refer to what expressed in response to (#2,11).

(#3;19):P.5, Section 3.2: See general comment above about estimates of condensed HNO_3 . I don't believe 20 ppb is reasonable.

Please refer to what commented on (#3;1).

(#3;20):P.5, L.460-464: How reasonable is the descent of the cloud from 17-14 km to 16.5- 13.5 in 6 days? What size particles and fall speeds would this correspond to? Is this consistent with the size distribution observed with the OPC? Does CALIPSO observe a similar vertical descent of the PSC? Is there any signature of reinitiation in MLS data at the lower altitudes after the PSC evaporated?

Fall speeds (Luo et al., 2003b) depend upon particle densities and dimensions (but also on shape, not taken into account) which are calculated by the microphysical model initiated by size distributions from OPC measurements. Hence there is an internal consistency between sizes and fall speeds. To present here a back of the envelope calculation, 100 m/day (approx. 10^{-3} m/s)) would correspond to spherical particles of approx. 1 μm diameter, so there is a good order of magnitude match with the observed and modeled particles. It is worth noting here that aspherical, or spongy, or NAT coated ice particles would have a different but basically unpredictable, fall speed (although recent studies (Woiwode et al., 2014), suggest a 30% reduction of NAT rocks fall speeds, to match with sedimentation observations carried out during the recent RECONCILE campaign). As noted in the first version of the manuscript, we did not have useful CALIOP matches when the PSC was present, as the closest match we presented is on the 15 September, when the PSC was vanishing. More relaxed matching criteria allowed us to use a match on 11 September 2008, discussed in the

answer to (#2,11). For what concerns signs of renitrification upon PSC evaporation, please refer to what exposed in answer to (#2,12).

(#3;21):P.6, L.512-519: This is true for all of the comparisons and should be discussed much earlier (e.g. Section 2.3). Can you elaborate more on how this may affect your analyses- does it limit your conclusions?

Sasano et al. (2000) and Terao et al. (2002) have used the Match approach in the Arctic based on ILAS satellite measurements, to compute ozone loss rates, and a similar Match study in Antarctica, based on POAM satellite data, has been reported by Hoppel et al. (2005). Match radii higher than the one used in our study (respectively 400 km for ILAS, and of 1000 km for POAM respectively) were used, and the problems due the relatively low vertical resolution and a large sampling air mass volume of the satellite sensors, leading imperfections in the matches (i.e., the re-sampled air mass is not identical, and the satellite data report a spatial average of the targeted specie) were reduced by computing ozone loss rates, based on a statistical analysis of many matches rather than a single pair. Obviously this approach cannot be pursued in our case, and the problem of satellite data averaged over their spatial resolution can only be reported. We have added at the end of paragraph 2.3, as suggested by the referee, the following lines:

“Although satellite data lacks the resolution and precision of in situ measurements, they have been used in the past for Lagrangian studies of the polar stratosphere (Santee et al., 2002, Sasano et al., 2000, Terao et al. ,2002, Hoppel et al.,2005, Riviere, 2003), relying on averaging observations and trajectory matches over long periods. As we are interested in a single case study, this standard approach cannot be used, and our comparison between modeled result and satellite observation will suffer from the inaccuracy due to the spatial averaging inherent to the satellite observations. The extent of this inaccuracy cannot be known a priori, but should be kept in mind when discussing our results.”

(#3;22):P.8, L.719-732: How dependent are your conclusions on the time scales and spatial scales of the case you've analyzed? Do you think the impact of denitrification on ozone depletion remains small over the course of the spring?

We have been trying to make clear that our conclusions are limited to this single case study, and the suggested message it drives should be that it may not be true that denitrification is ALWAYS important. Our study would suggest that there may be conditions under which this is not the case. Our study does not imply that the impact of denitrification is small or negligible over the course of the spring. This is now more explicitly stated in the revised text.

The new text: (32647,28-32648,4) “Although no general conclusion can be drawn from a single case study, our findings supports the view that there may be cases when additional surface area provided by solid PSC particles does not increase appreciably the chlorine activation, since in cold conditions the activation could originate from heterogeneous chemistry on surfaces basically provided by a background aerosol distribution.”

(#3;23):Figure 3: Much too small! I had to enlarge this significantly to even see the MLS and CALIPSO measurement locations and trajectories. This needs to be much larger.

Done.

(#3;24):*Technical P.6, L.546: “Groo” should be “Grooß.” P.6, L.568: “Groo” should be “Grooß.”*

This has been corrected.

(#3;25):*P.7, L.596-598: Citation is missing.*

The citation at the end of paragraph 3.3.1 is correctly present in the on-line version of our ACPD: Arnone et al., (2012).

(#3;26):*P.8, L.706: ‘as will be discussed later’ - is this really discussed ‘later’?*

We have changed the sentence in (32648,16) to:

“Moreover, although the effects of denitrification on HCl and ClONO₂ are opposite, so they cancel to some extent, the increase of ClONO₂ (not-denitrified vs. denitrified scenario: approx. 0.6 ppb by the end of the time interval) is larger than the decrease of HCl (approx. 0.2 ppb), so that in total more ClO_x is converted to reservoir species in the not-denitrified case.”

We have added the following references to the manuscript:

Hoppel, K., Bevilacqua R., Canty T., Salawitch R., Santee M. : A measurement/model comparison of ozone photochemical loss in the Antarctic ozone hole using Polar Ozone and Aerosol Measurement observations and the Match technique, *J. Geophys. Res.*, 110, D19304, doi:10.1029/2004JD005651, 2005.

Lambert, A., Santee, M. L., Wu, D. L., Chae, J. H.: A-train CALIOP and MLS observations of early winter Antarctic polar stratospheric clouds and nitric acid in 2008, *Atmos. Chem. Phys.*, 12, 2899-2931, doi:10.5194/acp-12-2899-2012, 2012.

Raspollini, P., Carli, B., Carlotti, M., Ceccherini, S., Dehn, A., Dinelli, B. M., Dudhia, A., Flaud, J.-M., López-Puertas, M., Niro, F., Remedios, J. J., Ridolfi, M., Sembhi, H., Sgheri, L., and von Clarmann, T.: Ten years of MIPAS measurements with ESA Level 2 processor V6 – Part 1: Retrieval algorithm and diagnostics of the products, *Atmos. Meas. Tech.*, 6, 2419-2439, doi:10.5194/amt-6-2419-2013, 2013.

Rivière E. D., A Lagrangian method to study stratospheric nitric acid variations in the polar regions as measured by the Improved Limb Atmospheric Spectrometer, *J. Geophys. Res.*, 108, D23, 2003.

Sasano, Y., Terao, Y., Tanaka, H.L., Yasunari, T., Kanzawa, H., Nakajima, H., Yokota, T., Nakane, H., Hayashida, S., Saitoh, N.: ILAS observations of chemical ozone loss in the Arctic vortex during early spring 1997, *Geophys. Res. Lett.*, 27(2), 213 – 216, 2000.

Schofield, R., Avallone, L. M., Kalnajs, L. E., Hertzog, A., Wohltmann, I., and Rex, M.: First quasi-Lagrangian in situ measurements of Antarctic Polar springtime ozone: observed ozone loss

rates from the Concordiasi long-duration balloon campaign, *Atmos. Chem. Phys.*, 15, 2463-2472, doi:10.5194/acp-15-2463-2015, 2015

Terao, Y., Sasano Y., Nakajima H., Tanaka H. L., Yasunari T., : Stratospheric ozone loss in the 1996/1997 Arctic winter: Evaluation based on multiple trajectory analysis for double-sounded air parcels by ILAS, *J. Geophys. Res.*, 107(D24), 8210, doi:10.1029/2001JD000615, 2002.

In this answer to referees' comments, we have quoted the following additional references:

Cairo, F., Di Donfrancesco, G., Snels, M., Fierli, F., Viterbini, M., Borrmann, S., and Frey, W.: A comparison of light backscattering and particle size distribution measurements in tropical cirrus clouds, *Atmos. Meas. Tech.*, 4, 557-570, doi:10.5194/amt-4-557-2011, 2011.

Carslaw, K. S., M. Wirth, A. Tsias, B. P. Luo, A. Dörnbrack, M. Leutbecher, H. Volkert, W. Renger, J. T. Bacmeister, and T. Peter: Particle microphysics and chemistry in remotely observed mountain polar stratospheric clouds, *J. Geophys. Res.*, 103(D5), 5785–5796, doi:10.1029/97JD03626, 1998.

Fueglistaler, S., Buss, S., Luo, B. P., Wernli, H., Flentje, H., Hostetler, C. A., Poole, L. R., Carslaw, K. S., and Peter, Th.: Detailed modeling of mountain wave PSCs, *Atmos. Chem. Phys.*, 3, 697-712, doi:10.5194/acp-3-697-2003, 2003.

Liu L., Mishchenko, M. I. : Constrains on PSC particle microphysics derived from lidar observations, *J. Quant. Spectrosc. Radiat. Transfer* , 70, 817-831, 2001.

Livesey N. J., Read, W. G., Froidevaux L., Lambert, A., Manney, G. L., Pumphrey H. C., Santee, M. L., Schwartz M. J., Wang S., Coeld R. E., Cuddy, D. T., Fuller, R. A., Jarnot, R. F., Jiang, J. H., Knosp, B. W., Stek P. C., Wagner, P. A., Wu, D. L.: Earth Observing System (EOS) Aura Microwave Limb Sounder (MLS) Version 3.3 and 3.4 Level 2 data quality and description document, Version 3.3x/3.4x-1.1, JPL D-33509, Jet Propulsion Laboratory California Institute of Technology Pasadena, California, 91109-8099, 2011.

Luo, B. P., C. Voigt, S. Fueglistaler, and T. Peter, Extreme NAT supersaturations in mountain wave ice PSCs: A clue to NAT formation, *J. Geophys. Res.*, 108(D15), 4441, oi:10.1029/2002JD003104, 2003a.

Luo, B. P., Peter, Th., Wernli, H., Fueglistaler, S., Wirth, M., Kiemle, C., Flentje, H., Yushkov, V. A., Khattatov, V., Rudakov, V., Thomas, A., Borrmann, S., Toci, G., Mazzinghi, P., Beuermann, J., Schiller, C., Cairo, F., Di Don-Francesco, G., Adriani, A., Volk, C. M., Strom, J., Noone, K., Mitev, V., MacKenzie, R. A., Carslaw, K. S., Trautmann, T., Santacesaria, V., and Stefanutti, L.: Ultrathin Tropical Tropopause Clouds (UTTCs): II. Stabilization mechanisms, *Atmos. Chem. Phys.*, 3, 1093-1100, doi:10.5194/acp-3-1093-2003, 2003b.

Rabier, F., Cohn, S., Cocquerez, P., Hertzog, A., Avallone, L., Deshler, T., Haase, J., Hock, T., Doerenbecher, A., Wang J., Guidard, V, Thépaut J-N., Langland,R., Tangborn, A., Balsamo, G., Brun, E., Parsons, D, Bordereau, J., Cardinali, C., Danis, F., Escarnot, J-P., Fourrié, N., Gelaro, R., Genthon, C., Ide, K., Kalnajs, L., Martin, C., Meunier, L-F, Nicot, J-M, Perttula, T., Potts, N.,

Ragazzo, P., Richardson, D., Sosa-Sesma, S., Vargas, A.: The Concordiasi Field Experiment over Antarctica: First Results from Innovative Atmospheric Measurements. *Bull. Amer. Meteor. Soc.*, 94, ES17–ES20, 2013.

Rex, M., von der Gathen, P., Harris, N. R. P., Lucic, D., Knudsen, B. M., Braathen, G. O., Reid, S. J., Backer, H. D., Claude, H., Fabian, R., Fast, H., Gil, M., Kyrö, E., Mikkelsen, I. S., 15

Rummukainen, M., Smit, H. G., Stähelin, J., Varotsos, C., and Zaitcev, I.: In situ measurements of stratospheric ozone depletion rates in the Arctic winter 1991/1992: a Lagrangian approach, *J. Geophys. Res.*, 103, 5843–5853, 1998.

Rex, M., Salawitch, R. J., Harris, N. R. P., von der Gathen, P., Braathen, G. O., Schulz, A., Deckelmann, H., Chipperfield, M., Sinnhuber, B.-M., Reimer, E., Alfier, R., Bevilacqua, R., Hoppel, K., Fromm, M., Lumpe, J., Kullmann, H., Kleinboehl, A., Bremer, H., von König, M., Kunzi, K., Toohey, D., Volmer, H., Richard, E., Aikin, K., Jost, H., Greenblatt, J. B., Loewenstein, M., Podolske, J. R., Webster, C. R., Flesch, G. J., Scott, D. C., Herman, R. L., Elkins, J. W., Ray, E. A., Moore, F. L., Hurst, D. F., Romashkin, P., Toon, G. C., Sen, B., Margitan, J. J., Wennberg, P., Neuber, R., Allart, M., Bojkov, B. R., Claude, H., Davies, J., Davies, W., De Backer, H., Dier, H., Dorokhov, V., Fast, H., Kondo, Y., Kyrö, E., Litynska, Z., Mikkelsen, I. S., Molyneux, M. J., Moran, E., Nagai, T., Nakane, H., Parrondo, C., Ravegnani, F., Skrivankova, P., Viatte, P., and Yushkov, V.: Chemical Depletion of Arctic Ozone in Winter 1999/2000, *J. Geophys. Res.*, 107, 8276, doi: 10.1029/2001JD000533, 2002.

Ricaud, B. Barrett, A. Kleinboehl, J. Kuttippurath, H. Kullmann, M. von Hobe, G.C. Toon, R.A. Stachnik: Validation of the Aura Microwave Limb Sounder ClO Measurements, *J. Geophys. Res.*, 113, D15S22, doi:10.1029/2007JD008762, 2008. Ridolfi M., S. Ceccherini, P. Raspollini, S. Niemeijer “Technical Note: Use of MIPAS vertical averaging kernels in validation activities”, Technical Note output of the ESA study “Support to MIPAS Level 2 product validation”, ESA-ESRIN Contract N. 17580/03/I-OL, 2010.

Rolf C., A. Afchine, H. Bozem, B. Buchholz, V. Ebert, T. Guggenmoser, P. Hoor, P. Konopka, E. Kretschmer, S. Müller, H. Schlager, N. Spelten, O. Sumińska-Ebersoldt, J. Ungermann, A. Zahn, and M. Krämer, Transport of Antarctic stratospheric strongly dehydrated air into the troposphere observed during the HALO-ESMVal campaign 2012 *Atmos. Chem. Phys. Discuss.*, 15, 7895–7932, 2015.

Santee M. L., A. Tabazadeh, G. L. Manney, M. D. Fromm, R. M. Bevilacqua, J. W. Waters, and E. J. Jensen A Lagrangian approach to studying Arctic polar stratospheric clouds using UARS MLS HNO₃ and POAM II aerosol extinction measurements *J. Geophys. Res.*, 107, NO. D10, 4098, 10.1029/2000JD000227, 2002

Santee, M.L., A. Lambert, W.G. Read, N.J. Livesey, G.L. Manney, R.E. Cofield, D.T. Cuddy, W.H. Daffer, B.J. Drouin, L. Froidevaux, R.A. Fuller, R.F. Jarnot, B.W. Knosp, V.S. Perun, W.V. Snyder, P.C. Stek, R.P. Thurstans, P.A. Wagner, J.W. Waters, B. Connor, J. Urban, D. Murtagh, P.

von der Gathen, P., M. Rex, N.R.P. Harris, D. Lucic, B.M. Knudsen, G.O. Braathen, H. De Backer, R. Fabian, H. Fast, M. Gil, E. Kyrö, I.S. Mikkelsen, M. Rummukainen, J. Stähelin, and C. Varotsos,

Observational evidence for chemical ozone depletion over the Arctic in winter 1991-92, *Nature*, 375, 131-134, 1995.

W. Woiwode, J.-U. Grooß, H. Oelhaf, S. Molleker, S. Borrmann, A. Ebersoldt, W. Frey, T. Gulde, S. Khaykin, G. Maucher, C. Piesch, and J. Orphal: Denitrification by large NAT particles: the impact of reduced settling velocities and hints on particle characteristics, *Atmos. Chem. Phys.*, 14, 11525-11544, 2014.

Lagrangian analysis of microphysical and chemical processes in the Antarctic stratosphere: a case study

L. Di Liberto¹, R. Lehmann², I. Tritscher^{3,6}, F. Fierli¹, J. L. Mercer⁴, M. Snels¹, G. Di Donfrancesco⁵, T. Deshler⁴, B. P. Luo³, J.-U. Groöß⁶, E. Arnone¹, B. M. Dinelli¹, and F. Cairo¹

¹Institute for Atmospheric Sciences and Climate, ISAC-CNR, Italy

²Alfred Wegener Institute, Potsdam, Germany

³Institute for Atmospheric and Climate Science, ETH Zurich, Switzerland

⁴Department of Atmospheric Science, University of Wyoming, Laramie, Wyoming, USA

⁵Ente per le Nuove Tecnologie Energia e Ambiente, Santa Maria di Galeria, Rome, Italy

⁶Institut für Energie und Klimaforschung - Stratosphäre (IEK-7), Forschungszentrum Jülich, Jülich, Germany

Correspondence to: F. Cairo (f.cairo@isac.cnr.it)

Abstract. We investigated chemical and microphysical processes in the late winter in the Antarctic lower stratosphere, after the first chlorine activation and initial ozone depletion. We focused on a time interval when both further chlorine activation and ozone loss, but also chlorine deactivation, occur.

We performed a comprehensive Lagrangian analysis to simulate the evolution of an air mass along a ten-day trajectory, coupling a detailed microphysical box model with a chemistry model. Model results have been compared with in situ and remote sensing measurements of particles and ozone at the start and end points of the trajectory, and satellite measurements of key chemical species and clouds along it.

Different model runs have been performed to understand the relative role of solid and liquid Polar Stratospheric Cloud (PSC) particles for the heterogeneous chemistry, and for the denitrification caused by particle sedimentation. According to model results, under the conditions investigated, ozone depletion is not affected significantly by the presence of Nitric Acid Trihydrate (NAT) particles, as the observed depletion rate can equally well be reproduced by heterogeneous chemistry on cold liquid aerosol, with a surface area density close to background values.

Under the conditions investigated, the impact of denitrification is important for the abundances of chlorine reservoirs after PSC evaporation, thus stressing the need of using appropriate microphysical models in the simulation of chlorine deactivation. We found that the effect of particle sedimentation and denitrification on the amount of ozone depletion is rather small in the case investigated. In the first part of the analyzed period, when a PSC was present in the air mass, sed-

imentation led to smaller available particle surface area and less chlorine activation, and thus less ozone depletion. After the PSC evaporation, in the last three days of the simulation, denitrification increases ozone loss by hampering chlorine deactivation.

1 Introduction

The depletion of ozone occurring in the polar stratosphere during winter and spring is linked to processes involving clouds in the polar stratosphere (Solomon et al., 1986). During winter the polar stratosphere cools to temperatures below 195 K, establishing a vortex circulation over the poles that separates the air inside from mid latitudes, and allows for the formation of Polar Stratospheric Clouds (PSC). Such clouds can be classified into three main particle types (Browell et al., 1990; Toon et al., 1990), Ia as solid trihydrates of nitric acid (NAT), Ib as supercooled ternary solutions of H₂O/HNO₃/H₂SO₄ (STS) growing by HNO₃ uptake by pre-existing stratospheric sulphate aerosol (SSA), type II as ice clouds, similar to tropospheric cirrus (Lowe et al., 2008). A new classification by Pitts et al. (2007, 2009, 2011) emphasizes that PSCs are often composed of mixtures of such particle types. PSC classifications have been critically reviewed in Achtert et al. (2014).

Extensive observations from ground-based as well as satellite instruments have provided climatologies of PSC occurrence in Antarctica (Adriani et al., 2004; Pitts et al., 2007; Di Liberto et al., 2014) and in the Arctic (Maturilli et al.,

2005). STS-NAT mixtures are the predominant composition classes of PSC observed throughout the stratosphere from mid-June until mid-September in Antarctica, with NAT particles prevailing at altitudes above 15 km (Pitts et al., 2009). Over McMurdo, PSC of prevalently NAT type appear in early June to achieve maximum occurrence in July at 20–24 km. The altitude of maximum occurrence has a downward trend from 24 to 14 km between July and September. PSCs become increasingly rare to non-existent after the middle of October. Their presence is widespread over Antarctica, although regions of enhanced occurrence are present above and eastward of the Antarctic Peninsula.

Heterogeneous chemical reactions taking place on or within PSC particles convert relatively non-reactive chlorine reservoir species such as ClONO₂ and HCl into active chlorine compounds as HOCl, ClNO₂ and Cl₂. Once the polar stratosphere has been primed by the action of heterogeneous chemistry on PSC particles, at the onset of spring the sunlight photolyses such compounds, releasing Cl which leads to catalytic ozone destruction.

Sedimentation of large PSC particles containing water and nitric acid causes dehydration and denitrification, depleting the stratosphere of water and nitric oxides that otherwise could reform chlorine reservoir species and reduce the lifetime of reactive chlorine. As the moderating effect of NO_x is missing, the considerable buildup of ClO drives the successive decrease in stratospheric ozone (Solomon, 1999).

The various kinds of PSCs influence such processes differently: the conversion of chlorine from less to more reactive species takes place with different efficiency, related to different PSC types (Biele et al., 2001; Carslaw et al., 1997; Tsias et al., 1999; Wegner et al., 2012); moreover, the sedimentation rate strongly depends on the average PSC particle size, which depends on its composition, phase and formation process.

In this paper, a case study of PSC evolution and its impact on ozone depletion and related processes in the late winter Antarctic stratosphere is presented. The study is based on in-situ and remote sensing observations of trace gases and particles, and Lagrangian microphysical and chemical models. After a first observation of PSC optical characteristics, particle size distributions and ozone taken over McMurdo Station (77° 51' S, 166° 40' E) by a set of balloon-borne in-situ instruments and a ground based lidar, the air mass has been tracked with a trajectory model until, after ten days, air in a certain altitude range returned to McMurdo within a distance of less than 300 km. Then a second in situ balloon sampling and lidar measurement was accomplished. Satellite measurements of key chemical species and particles along the air-mass trajectories documented its microphysical and chemical evolution. This dataset has been compared with simulations from chemical and microphysical box models reproducing the evolution of the cloud and evaluating its impact on the chemistry in the air mass. This well documented case took place in early September, soon after the onset of ozone depletion

from chlorine activation but before complete destruction of ozone, in a region close to the vortex edge. By modeling the microphysical and chemical processes along the trajectory and comparing simulations with observations, an assessment of the modeled denitrification, ozone chemistry, and the impact of PSC occurrence on ozone depletion can be made. Finally, an evaluation of the relative importance of the heterogeneous chemistry and denitrification will be made. The scope of this study is to provide a contribution to the most recent discussion of the relative role of PSC and liquid (background) aerosol in the ozone depletion (Drdla and Müller, 2012; Wegner et al., 2012; Wohltmann et al., 2013).

2 Instruments and Models

2.1 In Situ Instruments

Balloon-borne instruments have been routinely launched from McMurdo Station since the 1980s (Mercer et al., 2007). Balloons are routinely equipped with instruments to measure ozone (Deshler et al., 2008), temperature, pressure and humidity, and occasionally with Optical Particle Counters (OPC) (Hofmann and Deshler, 1991; Adriani et al., 1995; Deshler et al., 2003b).

Ozone measurements are performed with commercial electrochemical cell (ECC) ozonesondes, developed and described by Komhyr (1969). A Vaisala radio sonde RS92 performs pressure, temperature and humidity measurements using sensors designed to cover all atmospheric and weather conditions in every climate zone. The model RS92 provides temperature and pressure with an accuracy respectively of 0.25 K and 0.2 hPa near 50 hPa (Steinbrecht et al., 2008).

The OPC counts and sizes particles drawn into a sampling chamber. The single particle instrument uses white light scattering at 40° in the forward direction to measure size using Mie theory. Deshler et al. (2003a) have described the measurement principles and their inherent uncertainties in significant detail, concluding that the uncertainties in size are in the range of 10% for most sizes, while concentration errors range from 8 to 80 % for low concentrations. The impact of these uncertainties on integrals of the size distribution, such as surface area, are on the order of ±40%.

2.2 Ground based lidar

McMurdo Station has been hosting a polarization diversity Rayleigh lidar since 1991 (Adriani et al., 2004), which was upgraded in 2004 (Di Liberto et al., 2014). The Backscatter Ratio, defined as the ratio of the total backscattered light to the one expected from an atmosphere free of aerosol, is retrieved by using the Klett algorithm, with an extinction-to backscatter ratio (lidar ratio) calculated using the empirical model proposed by Gobbi et al. (1995). The ratio of the parallel to the cross polarization signals, the volume depolarization ratio δ , is used to detect the presence of non spher-

ical (i.e. solid) aerosol. This quantity is calibrated with the method described by Snels et al. (2009). The Aerosol Depolarization Ratio δ_a , retrieved from δ by eliminating the molecular contribution from the backscattering (Cairo et al., 1999), is a more direct characterization of the particle morphology, and is here presented. The uncertainty affecting these optical parameters has been estimated following the method reported in Russell et al. (1979) and is 0.1 (in absolute value) or 10% of the measured value (the larger of the two) for the aerosol backscatter ratio (BR-1) and 3% (in absolute value) or 10% of the measured value (the larger of the two) for the aerosol depolarization.

2.3 Satellite instruments

The Aura Microwave Limb Sounder (MLS) measures thermal emission continuously (24 hours per day) using a limb viewing geometry which maximizes signal intensity and vertical resolution. Vertical profiles of mixing ratios of many different chemical species, temperature and pressure are derived (Waters et al., 2006). The MLS results for stratospheric ozone have been extensively validated and are in good agreement with other datasets from many different origins (Froidevaux et al., 2006). Ozone vertical profiles have vertical resolution of approximately 3 km from 215 hPa to 0.2 hPa and about 4–6 km between 0.2 and 0.1 hPa. The ozone precision is 0.04 ppmv in the range 215–68 hPa, 0.1–0.4 ppmv in the range 46–0.1 hPa and 1–0.06 ppmv between 0.05 and 0.02 hPa. The vertical resolution for the standard HCl product is 3 km in the stratosphere. The estimated single-profile precision reported for the Level 2 product varies from 0.2 to 0.6 ppbv in the stratosphere. HNO₃ data are reliable over the range 215 to 3.2 hPa, with a vertical resolution of 3–4 km in the upper troposphere and lower stratosphere. The precision is approx. 0.6–0.7 ppbv throughout the range from 215 to 3.2 hPa (Santee et al., 2007). MLS ClO profiles have a vertical resolution of 3 km in the altitude range of interest for our study, and v2.2 data are reported with a precision of 0.1 ppbv in the range 100–3 hPa. H₂O profiles have a vertical resolution of about 2–3.5 km in the range 316–0.22 hPa, a precision of 6–8 % and accuracy of 4–6 %. In the region and altitude of interest, MLS horizontal resolutions in along-track direction are reported to be of the order of 200–300 km for most targets (including H₂O, 400–500 km for ClO), cross-track resolution is approx. 3 km, and the separation between adjacent retrieved profiles along the measurement track is 1.5 great circle angle (approx. 165 km). Further information on the MLS instrumentation and its products can be found at: <http://mls.jpl.nasa.gov/>.

In our study we have used MLS data in their version 2.2 generated by the GIOVANNI data analysis web application. We have considered MLS profiles when the MLS overpass was included in a box of $\pm 2^\circ$ lat and $\pm 15^\circ$ lon with a time difference less than 12 hours with respect to the airmass location along its trajectory. MLS data (delivered on pressure

levels) were interpolated to find the mixing ratio at the isentropic levels (or altitudes) of our interest. This has been done by identifying the pressure value at the isentrope (or altitude) of interest from our radiosoundings, then linearly interpolating the MLS data in term of logarithmic pressures.

MIPAS (Michelson Interferometer for Atmospheric limb Sounding) measured the upper tropospheric and stratospheric composition from a polar orbit on board the ESA ENVISAT satellite from 2002 to 2012 (Fisher et al., 2008). MIPAS was a limb-scanning Fourier Transform interferometer that measured emission spectra in the thermal infrared, on a wide spectral range (680 to 2410 cm⁻¹). We adopted MIPAS data from the MIPAS2D database (Dinelli et al., 2010), (<http://www.isac.cnr.it/~rss/mipas2d.htm>) retrieved with the GMTR (Geo-fit Multi-Target Retrieval) analysis tool (Carlotti et al., 2006). The vertical resolution of MIPAS2D data is about 4 km for the altitude range of interest of this paper. MIPAS along track sampling step is about 410 km. The width of the Field Of View at tangent point in the cross-track direction is about 30 km. The smearing of information around the tangent point given by the width of the single scan horizontal averaging kernels is 200–300 km, for most species (Raspollini et al., 2013). However, the MIPAS products used here are obtained by a 2-D (along track) analysis code, and its horizontal resolution is limited by the 410 km sampling step adopted in the retrievals. Total systematic errors at the altitudes of interest for this study are: 3–8 % for pressure, 0.7–1.5 K for temperature, 5–7 % for ozone, and 5–20 % for the other species. Random errors are: 0.5–1.5 % for pressure, 0.2–0.3 K for temperature, 2–5 % for ozone, 2–10 % for the other species. We have considered MIPAS profiles when the overlap of the MIPAS overpass was included in a box of $\pm 2^\circ$ lat and $\pm 15^\circ$ lon with a time difference less than 12 hours with respect to the airmass location along its trajectory. Potential temperatures were self-consistently calculated from pressure and temperature, and the selected MIPAS2D profiles interpolated at the potential temperature level of the models.

The Cloud-Aerosol Lidar with Orthogonal Polarization (CALIOP) is a two-wavelengths (532 and 1064 nm) lidar, with two polarizations at 532 nm, on board the CALIPSO (Cloud-Aerosol Lidar and Infrared Pathfinder Satellite Observation) satellite which provides vertical profiles of aerosols and clouds, and has been extensively used for studies on PSC (Pitts et al., 2007, 2009, 2011). It has a vertical resolution between 30 m and 60 m and a horizontal resolution of 333 m and 1 km for altitudes between 0.5 km and 8.2 km and between 8.2 and 20.2 km, respectively. The CALIPSO satellite is part of the A-Train track (Stephens et al., 2002). Since early 2008 CALIOP and MLS make measurements within about 30 s of one another. MLS profiles are separated by about 165 km along the orbit, while CALIPSO samples on a much finer horizontal resolution of approx. 1 km in the lower stratosphere (Lambert et al., 2012) and performs measurements on the same MLS geo locations, only some few minutes later. In this work we considered

CALIOP profiles collected during night time and matching the $\pm 1.0^\circ$ Latitude, $\pm 2.5^\circ$ Longitude, ± 12 hour time difference criteria, with respect to the traced air mass location. More information on CALIOP can be found at <http://www-calipso.larc.nasa.gov/>.

Although satellite data lacks the resolution and precision of in situ measurements, they have been used in the past for Lagrangian studies of the polar stratosphere (Santee et al., 2002; Sasano et al., 2000; Terao et al., 2002; Hoppel et al., 2005; Riviere et al., 2003), relying on averaging observations and trajectory matches over long periods. As we are interested in a single case study, this standard approach cannot be used, and our comparison between modeled result and satellite observation will suffer from the inaccuracy due to the spatial averaging inherent to the satellite observations. The extent of this inaccuracy cannot be known a priori, but should be kept in mind when discussing our results.

2.4 Trajectory model

During the field campaign, the air parcel trajectories were tracked by using the Goddard Space Flight Center (GSFC) isentropic trajectory model (http://acdb-ext.gsfc.nasa.gov/Data_services/automailer/index.html). In the course of the data analysis, and for the purposes of this study, additional trajectory tools have been used for checking the results of the field campaign. For the purpose of microphysical modelling, the air parcel trajectories have been recalculated by the trajectory module of CLaMS (Chemical Lagrangian Model of the Stratosphere) using 6 hourly ERA-Interim (Dee et al., 2011) wind and temperature fields with a horizontal resolution of $1^\circ \times 1^\circ$. CLaMS is a modular chemistry transport model (CTM) system developed at Forschungszentrum Jülich, Germany (McKenna et al., 2002a, b; Konopka et al., 2004). Integration of trajectories has been accomplished with an integration time step of 15 minutes. Vertical displacements of isentropic trajectories are derived from ERA-Interim total diabatic heating rates (Plöger et al., 2010). CLaMS produced forward trajectories from the time and location of the first PSC observation, starting on 10 Sep 2008 at 12:00 UTC. The vertical spacing between the trajectories is about 100 m in a vertical range between 350 and 450 K. The GSFC and CLaMS trajectories document similar paths travelled by the air mass, although wind speed was slightly lower during the first days of the simulation in the ERA Interim dataset.

2.5 Microphysical and optical model for PSC

The Zurich Optical and Microphysical box Model (ZOMM) has been developed for PSC simulations to study the formation, growth and evaporation of PSC particles determined by changes in temperature and pressure. ZOMM includes the following PSC formation pathways: Liquid background particles grow into STS droplets by uptake of HNO_3 (Dye et al.,

1992; Carslaw et al., 1995). Ice nucleation takes place either homogeneously at sufficiently low temperatures (Koop et al., 2000) or heterogeneously on the surfaces of foreign nuclei (Engel et al., 2013). NAT nucleation is implemented as heterogeneous nucleation on foreign nuclei (Hoyle et al., 2013) as well as on uncoated ice surfaces (Luo et al., 2003).

Small-scale temperature fluctuations, that are required to accurately reproduce ice number densities, are superimposed onto the synoptic-scale trajectories. The sedimentation of PSC particles is accounted for by using the column version of ZOMM as described in Engel et al. (2014). So far, ZOMM has always been initiated at typical background conditions for the winter polar stratosphere (Hoyle et al., 2013; Engel et al., 2013). The study by Engel et al. (2014) was the first study, which used the microphysical model as a column model for PSC simulations. For the present study, we developed the model further and introduced the possibility to prescribe a particle size distribution. We extracted those data from the OPC measurements taken at the trajectory starting points and complemented the condensed amount of H_2O and HNO_3 with gas phase values measured by MLS. The optical output, calculated using Mie and T-Matrix scattering codes (Mishchenko et al., 2012) can directly be compared to CALIOP measurements. The calculated surface area of PSCs along the trajectories serves as input for the chemistry model. Using a box model such as ZOMM for PSC studies allows a detailed microphysical calculation of cloud processes, which cannot be achieved with global models due to limited computing resources. Case studies without wind shear, as often observed in the polar vortex, offer the possibility to run ZOMM as a column version and, by doing this, to simulate also the vertical redistribution of particles.

2.6 Chemistry model

The temporal evolution of the mixing ratios of chemical species along trajectories was simulated by the Alfred Wegener Institute chemical box model. It contains 48 chemical species and 171 reactions, describing the stratospheric chemistry. It is based on a module for gas-phase chemistry described in Brasseur et al. (1997) and a module for heterogeneous chemistry reported in Carslaw et al. (1995). Reaction rate constants have been updated to the values given by Sander (2011). For these simulations, the initial mixing ratios of ClO , HCl , HNO_3 , CO , N_2O , H_2O , and O_3 were taken from the nearest MLS and ozonesonde measurements. The mixing ratios of NO_x (NO , NO_2) and ClONO_2 were assumed to be close to zero in agreement with the MIPAS ClONO_2 observations. Inspection of MLS maps for H_2O , HNO_3 , ClO , O_3 , HCl , N_2O available at 56 hPa level at http://mls.jpl.nasa.gov/plots/mls/mls_plot_locator.php for 10 September 2010, shows relatively low meridional gradients of the species of interest over McMurdo, thus giving confidence on the low spatial variability of the values used to initialize our model calculations. To start with balanced ini-

365 tial values, pre-runs of the chemical box model on a one day
back-trajectory ending at the start point of the correspond-
ing main trajectory were performed. The initial mixing ratios
for these pre-runs were iteratively modified, until the MLS
measurements were reproduced by the model at the end of 420
370 the pre-run trajectory. Then the mixing ratios of all species at
the end of the pre-run were used as initial values for the run
of the chemical box model on the main trajectory. As part
of this procedure, a ClO_x ($= \text{ClO} + 2 \cdot \text{Cl}_2\text{O}_2$) mixing ratio
consistent with the MLS ClO measurement was determined, 425
375 which is essential for a correct simulation of the chemical
ozone depletion.

3 Observations and Simulations 430

3.1 McMurdo observations

A balloon carrying an OPC and an ozone sonde was launched
380 from the Antarctic station of McMurdo on 10 September 2008,
10:55 UTC. Lidar measurements were simultaneously made
during the 4 hours duration of the balloon flight. A PSC was
observed for 70 minutes in the initial part of the flight,
during ascent, over a horizontal distance of ~ 50 km.
385 The left panel of Fig. 1 depicts the lidar backscatter (solid
line) and aerosol depolarization (dotted line) ratios vs. alti-
tude, averaged over the OPC observation time, while the right
panel shows the particle size distribution measurements ob-
tained by the OPC. A layered PSC can be clearly discerned
390 between 11.5 and 17.5 km (~ 330 -420 K potential temper-
ature). The lowermost layer shows small Backscatter Ratio
values, but significant depolarization around 30%, typical of
NAT PSCs. The two layers between 14 (~ 360 K) and 17 km
show a higher Backscatter Ratio of about 3 and 2.5, depo-
395 larization around 40%, again characteristic values for NAT
PSCs. The particle size distribution confirms this classifica-
tion, particles above $1 \mu\text{m}$, typical of NAT particles (Voigt
et al., 2000) reaching concentrations of up to 10^{-1} cm^{-3} .
Temperatures (not shown) were above the ice freezing tem-
400 perature T_{ice} all along the profile. 455

Backtrajectory analysis showed that in the 10 days preced-
ing the observation, the air in which the PSC was detected
remained south of 60° S, its temperature going below 195K
on 4 September, reaching 182K the subsequent day and then
405 hovering around 190K for the days prior to our observation. 460

The red solid line in Fig. 2 shows the measured ozone
profile in the 300-500 K potential temperature range, cor-
responding approximately to altitudes between 10 km and
20 km. The ozone values on 10 September fall within the
410 climatological variability reported in Kröger et al. (2003) at
the onset of the mid-September ozone depletion. During the
campaign, we tracked the air mass sampled by the in-situ in-
struments with the GSFC trajectory model finding that after
approximately 10 days the air between 380 and 420 K po-
415 tential temperature (where the PSC was observed) returned 470

over the Ross Sea less than 300 km from McMurdo. A sec-
ond balloon sounding was performed on 20 September 07:30
UTC, to match the return of the air mass close to the 400K
level. During this second balloon sounding, and in the 24
hours preceding it, lidar measurements (not shown) showed
no sign of PSCs. The ozone profile, in Fig. 2 with a blue solid
line, showed reduced values between 360 and 420 K (14
and 17 km), in the altitude region where the PSC was ob-
served ten days earlier. There, the ozone was reduced from
500-600 ppbv to 100-200 ppbv on average. Very different ozone
values between the two samplings are also discernible in the
uppermost part of the sounding between 420 and 500 K (above
17 km up to 20 km). The gray area in Fig. 2 marks the alti-
tude region where the air mass reencounter was expected.
There, the two profiles show a similar depression with mini-
430 ma at 405 K. In that region, the ozone decrease between the
two soundings is about 300 ppbv below 405 K, a little more
above.

These ozone losses are comparable with what was ob-
served in the past (Mercer et al., 2007; Kröger et al., 2003;
Nardi et al., 1999) in the same period of the year. The double
overpass of the air mass over McMurdo in the layer between
380 K and 420 K suggested a detailed Lagrangian study of
the microphysics and chemistry that occurred in the air mass,
between the two balloon observations.

In the left panel of Fig. 3, isentropic air mass trajec-
tories, starting from McMurdo on 10 September 2008 12 UTC
are shown (color coded according to potential temperature).
Solid/dotted portions of the lines designate the sunlit/dark
sectors of the trajectories. The right panel reports tempera-
ture histories along those trajectories (again color coded in
term of their potential temperature). The trajectories in the
375-425 K layer remained confined within the vortex and
show a limited variability in PV (not shown). Air masses
close to 400 K level returned over McMurdo after approx-
imately 9.5 days. In those air masses, the PSC was observed
on 10 September and temperatures remained below 195 K
for the initial five days of the trajectory. Then the air masses
experienced a warming in the second part of the trajectory.

To compare the results of our model simulations with ob-
servational data along the path of the air mass, coincidences
between the air mass trajectory and CALIOP and MLS obser-
vations were determined. In the leftmost panel of Fig. 3, pur-
ple dots indicate availability of MLS data, and purple lines
crossing the trajectories specify intersections with CALIOP
440 footprint.

Figure 4 shows longitude vs altitude curtains of Backscatter
Ratio from CALIOP nighttime footprints crossing the air-
mass trajectory at various stages of its evolution. Red circles
indicate the intersection of the curtain with the 400 K isoen-
tropic trajectory. CALIOP data document the presence of a
large PSC observed between 15 and 17.5 km on Septem-
ber 14 (daytime footprint, not shown), with values of the
optical parameters which are the same order of magnitude
of those observed above McMurdo four days earlier. On the

next day, the top of a weak PSC is present in the region intersected by the air trajectory. Its shape resembles the previous day's observations. On the night of 16 September the PSC is almost completely dissipated and vanishes in the following days. The CALIOP depolarization (not shown) indicates that observations are consistent with a dominantly NAT PSC. The CALIOP observations document a large PSC in the area crossed by the trajectory of the airmass which was sampled five days earlier by the in situ aerosol measurements from McMurdo.

3.2 Microphysical simulations

The microphysical model was initialized with MLS H₂O and HNO₃ profiles closest in time and space to the first McMurdo balloon sounding. Since those values are gas phase values only, the amount of HNO₃ taken up by existing STS droplets and NAT particles at the time of the PSC observation had to be computed. For those calculations we made use of the size distribution measured by the balloon-borne OPC. The smallest size bins up to 0.75 μm were considered to consist of STS droplets with a density of 1.44 g cm⁻³. Larger particles of the OPC size distribution were taken as NAT particles and the condensed HNO₃ phase was computed by assuming spherical NAT particles with a density of 1.62 g cm⁻³. With these assumptions estimates of HNO₃ content in the particles larger than ~ 0.3 μm ranged from 20-30 ppbv from 370-385 K (14.5-15.5 km), to near 10 ppbv from 385 - 405 K (15.5-16.8 km). While these values are higher than expected, they result from the OPC measurements of significant concentrations (~ 0.1 cm⁻³) of particles in the 2-3 μm range, so are not easily dismissed. A possible overestimation of the HNO₃ content in the condensed phase from particle size measurements was reported in some recent airborne measurements from the RECONCILE campaign (von Hobe et al., 2013) and possible reasons for that are extensively discussed in Molleker et al. (2014). The microphysical run was initialized with an estimate of the initial value of total HNO₃ of 6.9 ppb, of which 5.2 ppb in condensed phase, considered as a realistic upper limit for the amount of HNO₃ in the particles. Results from this run will be presented here. The OPC size distribution was also used to prescribe existing NAT particles at the starting point of the trajectories. Temperature and pressure along the trajectories computed with the CLaMS trajectory module were used as input to predict the PSC evolution.

Figure 5 shows the modeled evolution of the PSC in terms of Backscatter Ratio (upper panel), Aerosol Depolarization (middle panel) and total HNO₃ (lower panel) during the 10-20 September period. The persistence of the PSC for almost a week is evident. The cloud remains of NAT type for 6 days after the first McMurdo balloon sounding, and totally evaporates three days before the second McMurdo sounding, as a warming caused its disappearance before 16 September. This warming in the second part of the trajectory coincides with

an increasing distance of the airmass from the vortex centre. A vertical redistribution of the cloud is also evident, caused by the modelled particle sedimentation. The cloud vertical extent changes from 410-360 K (~ 17-14 km in geometrical altitude) to 390-350 K (~ 16.5-13.5 km) in 6 days. A large vertical redistribution of the gas phase HNO₃ can be seen after the evaporation of the PSC. This occurrence has been confirmed by MLS HNO₃ data on locations along the 400K trajectory.

3.3 Chemical simulations

Chemistry model runs were performed along the CLaMS trajectories. Although the model has a microphysical module, it was forced to use prescribed values of HNO₃ (total and gas phase), STS/SSA and NAT aerosol surfaces, as provided offline by the microphysical model output. This is because only the microphysical model could take into account particle sedimentation. The calculations were stopped at the trajectory point closest to McMurdo.

3.3.1 Effects of heterogeneous chemistry

Two model runs were performed, respectively with and without the inclusion of heterogeneous chemistry. We hereafter present results of the simulations at the 400 K isentropic level, in the middle of the altitude region of the airmass trajectory match. As shown in Fig. 2, a trough in the ozone profile at 400 K implies that ozone depletion has markedly occurred already before the time of the first sounding. This isentropic level is close to the upper limit of the PSC observed on 10 September, so it is where the consequences of particle sedimentation and HNO₃ redistribution were likely to be more pronounced, as the microphysical simulation shows in Fig. 5, reporting profiles of Backscatter Ratio and Aerosol Depolarization. At 400 K, the NAT particle surface area decreased steadily from an initial value of 4.5 μm² cm⁻³ to 0 in 100 hours, while STS/SSA particle surface area hovered around 1.5 μm² cm⁻³ throughout the simulation, a value not far from what expected for the background aerosol surface area density (Hitchman et al., 1994; Chayka et al., 2008).

Figure 6 reports the results of the chemistry simulations, with (red line) and without (blue line) heterogeneous chemistry taken into account. Yellow regions represent sunlit parts of the trajectory. Figure 6 a) reports O₃ evolution. Removing heterogeneous reactions leads to less chlorine (re-)activation and, consequently, less ozone loss. However, the effect is not very strong, because most of the chlorine is already activated at the beginning of the trajectory, according to MLS data. Squares represent ozone measured by MLS along the trajectory. There, and in the following panels, the radius of the circles surrounding the data points represents the match radius, defined as the distance between the observation and the location of the airmass on its trajectory, at the time of the

575 observation. The simulations capture the integrated ozone 630
loss well, although intermediate comparisons are not good,
as the large depletion is delayed in the observations until after
15 September. Such behavior should not be expected in the
present case, where both ClO_x and sunlight are available for
580 ozone depletion throughout the whole period. In the compar- 635
ison with the measurements, however it has to be taken into
account that positions of the satellite measurements and cor-
responding trajectory points do usually not coincide. More-
over, limb soundings represent averages over large horizontal
585 distances, and therefore might not have been able to fully ac- 640
count for processes going on in a relatively small portion of
air.

HNO_3 concentrations both total and gas phase were not
calculated by the chemistry model, but prescribed by the mi-
590 crophysical model. Figure 6 b) reports the evolution of the 645
modelled HNO_3 in the gas phase, driven initially by PSC
particle condensation and successive evaporation after a ver-
tical redistribution and removal due to particle sedimentation.
Squares and stars represent respectively MLS and MIPAS
595 data. In this case the agreement between simulation and ob- 650
servation seems reasonable although the measured uncertain-
ties are large and the MIPAS and MLS scarcely agree with
each other, with the MLS more consistent with the model.
The microphysical model seems to well reproduce both the
600 HNO_3 sequestering in condensed phase until 14 September, 655
and then some denitrification. Note again that sedimentation
processes are very localized and their effects are observed by
satellites only if the effects cover a large area.

Heterogeneous chemistry affects the evolution of HCl
605 (Fig. 6 c)) and ClONO_2 (Fig. 6 d)) respectively. As long 660
as the PSC is present, both species are reduced by heteroge-
neous reactions. MLS HCl values are reported as squares and
MIPAS ClONO_2 are reported as stars.

The comparison with the observed values seems to sug-
610 gest that the simulation with heterogeneous chemistry active 665
is more effective in reproducing the HCl evolution over the
studied period. However, as the speed of Cl deactivation is
sensitively dependent on ozone mixing ratios (Douglass et
al., 1995; Grooß et al., 1997, 2011), but the ozone compar-
615 ison is not fully satisfactory, it is difficult to interpret this
HCl and ClONO_2 comparison. In order to estimate how sen-
sitively HCl depends on the accuracy of ozone mixing ratio 670
evolution in the present case, an additional sensitivity model
run was then performed under the rather extreme assumption
620 that there is no ozone depletion at all (i.e. by holding constant
the ozone mixing ratio to its initial value throughout the sim- 675
ulation). Results of this sensitivity run are reported as a green
solid line. The induced change in the HCl evolution is not too
large, and HCl mixing ratios of the sensitivity run are still
625 compatible with the MLS measurements between September
12 and 17.

A closer look at the reactions affecting ozone and HCl is 680
presented in Fig. 7, reporting the O_3 depletion rates due to
the ClO-BrO and ClO-ClO catalytic cycles (left panel) and

the HCl production and destruction rates (right panel) due to
a set of competing reactions listed at the bottom of the figure.
Ozone is mainly destroyed by the ClO dimer and the ClO-
BrO catalytic cycles. No noticeable ozone production is tak-
ing place. Most of the chlorine activation is accomplished by
the reaction of HCl with HOCl (both on NAT and STS/SSA),
which is a result consistent with Grooß et al. (2011). There is
a short time window (between 14 and 15 September) when
also the reaction of HCl with ClONO_2 on STS/SSA is con-
tributing. Before that period the ClONO_2 concentration is
rather low, as reported in Fig. 6 d), because most of the nitro-
gen is in NAT particles. After that period the temperature is
higher and thus the rate of the temperature-dependent reac-
tion of ClONO_2 with HCl on liquid aerosol is smaller. In the
model run, during the first days both NAT and liquid aerosol
particles contribute to chlorine activation. After the sedimen-
tation prevents further NAT particle existence, the reactions
on liquid particles obviously prevail.

To further explore the relative role of NAT and STS/SSA,
the model was run by separately switching on the heteroge-
neous reactions on NAT or on STS/SSA alone.

Figure 8 shows the O_3 evolution with full heterogeneous
chemistry (red), or with only heterogeneous chemistry on
NAT (green) or on STS/SSA (blue). Although the heteroge-
neous reactions on NAT particles contributed to the chlorine
activation during the first days (as shown in Fig. 6 a)), in our
study STS/SSA particles might have been effective on their
own to produce the observed depletion occurred in 10 days
after 10 September. Although a single case study does not al-
low to express any general statement for ozone depletion in
the whole winter, our conclusion is in line with the results by
Drdla and Müller (2012) (Arctic and Antarctic) and Wegner
et al. (2012) and Wohltmann et al. (2013) (Arctic), who ar-
gue that cold liquid aerosols alone could provide most of the
chlorine activation. A major role of STS particles in driving
the extreme ozone reduction in the Arctic 2011 was found by
Arnone et al. (2012).

3.3.2 Effects of particle sedimentation

As the influence of PSCs on chemistry is twofold, provid-
ing the surface for heterogeneous reactions and removing ni-
trogen compounds by sedimentation (denitrification), an ad-
ditional chemistry model run was performed to obtain an
estimation of the effect of the denitrification on the chem-
istry. This was done by providing new microphysics con-
straints, obtained by performing a new run of the microphys-
ical model that did not account for particle sedimentation.
In such configuration, a PSC was produced between 365 K
and 410 K, remaining in this vertical range for 5 days, before
subsequent warming caused its evaporation.

Results of this model run are depicted in Fig. 9 which re-
port the time evolution of ClONO_2 (Fig. 9 a)), HCl (Fig. 9
b)) and O_3 (Fig. 9 c)). Red curves report simulations with
sedimentation and blue curves report simulations with no

sedimentation. The effect of sedimentation (denitrification) is not very large, but still detectable. In the first phase, until 16 September when temperatures were low enough for the existence of the PSC, the lack of particle sedimentation in the microphysical model allowed NAT surfaces at 400K to remain high, leading to enhanced chlorine activation, and enhanced ozone loss. After 15 September, the temperature became too high for NAT existence, significantly decreasing the rates of the heterogeneous reactions on aerosols, and chlorine activation stopped. In absence of denitrification after PSC evaporation more chlorine is deactivated, the growth of HCl decreases by a factor 2, and similarly the buildup of ClONO₂ increases by a factor 4, as more NO₂ is available so that, from the moment of PSC evaporation on, the absence of denitrification causes slightly less ozone depletion rates. The final amount of HCl is reduced with respect to the denitrified scenario, and that is the result of different and counteracting effects. During the PSC existence, more HCl is destroyed in heterogeneous reactions with HOCl and ClONO₂, as more NAT surface is available. After the PSC evaporation, the ClO and OH mixing ratios are smaller in the not-denitrified scenario, because more NO₂ and HNO₃ are available to convert ClO_x and HO_x species to the reservoirs ClONO₂ and H₂O via the reaction of ClO and NO₂ to produce ClONO₂, and OH with HNO₃ to produce H₂O and NO₃. That is why the HCl production by the reaction of ClO with OH is reduced. A counteracting effect results from a shift in the ClO_x partitioning: Cl is enhanced by the reaction of ClO and NO, that produces NO₂ as well, resulting in an increased HCl production by the reaction of Cl with CH₄.

4 Conclusions

An in-situ observation of an air mass when a PSC was present, by an optical particle counter and ozonometer on a balloon launched from the Antarctic station of McMurdo, where a polarization diversity lidar was also operating, provided information on PSC characteristics and ozone abundance. A trajectory analysis revealed that the air mass at around the 400K level was close to McMurdo Station ten days later, when lidar and ozone sounding were accomplished, showing a marked ozone depletion and no sign of PSCs. The McMurdo in situ measurements were complemented by O₃, HCl, ClONO₂ and HNO₃ observations from the satellite-borne MLS and MIPAS instruments and by particle observation from the satellite-borne CALIOP lidar, taken along the air mass trajectory connecting the two McMurdo overpass measurements. The observations have been compared to microphysical and chemical box models, run along the air mass trajectory, to investigate the evolution of the PSC and the sensitivity of the modelled chemistry to its presence. The detailed microphysical box model reproduces the evolution and type of PSC, as documented by the CALIOP observations along the air mass trajectory. The mag-

nitude of ozone depletion was well captured by the chemical model, as were the evolution of the reservoir species HCl and ClONO₂. In our case study, ozone destruction processes were investigated at a time when there was already a significant amount of activated chlorine at the beginning of the simulations, and there was ozone depletion already before the time window analyzed. This probably explains why, in this case, along the trajectory investigated the effect of heterogeneous chemistry on ozone depletion was not very large, accounting for a difference of less than 8 ppb/day in the overall modeled ozone depletion rate of 35 ppb/day, in fair agreement with an ozone loss of ~ 30 ppbv/day that can be deduced from the balloon data. We should note that the value of the modeled ozone loss rate is within the ranges reported in the literature (Schofield et al., 2015) and the difference between its value whether heterogeneous chemistry on PSC particles has been considered, or not, is beyond both its reported atmospheric variability, and the sensitivity of our measurements. As long as a NAT PSC existed (i.e. in the first half of the time interval investigated), it contributed to the chlorine activation. However, according to our findings, under the conditions investigated, the liquid aerosols with assumed surface area densities not far from stratospheric aerosol background values, could produce the observed chlorine activation alone. Although no general conclusion can be drawn from a single case study, our findings supports the view that there may be cases when additional surface area provided by solid PSC particles does not increase appreciably the chlorine activation, since in cold conditions the activation could originate from heterogeneous chemistry on surfaces basically provided by a background aerosol distribution. As expected, differences arising from the presence of particles (whether background aerosol or PSC) and from heterogeneous chemistry that they allow, are more remarkable when gas phase chlorine reservoirs are examined. In fact, the buildup of HCl and, particularly, of ClONO₂ is significantly reduced by heterogeneous reactions. Turning our attention to the effect of denitrification on ozone depletion at 400 K, at the top of the observed PSC, we came to the conclusion that, in our study, this effect is small. In this case this may be due to two opposite effects of denitrification (and the length of the time sub-intervals in which either of these effects is dominant): 1) a reduction of the NAT surface area density and thus of their contribution to chlorine activation, and consequently of the ozone loss during the first 5 days of the simulation; 2) a counteracting reduction of chlorine deactivation and thus an increase of the ozone loss during the last 3 days of the simulation. Moreover, although the effects of denitrification on HCl and ClONO₂ are opposite so they cancel to some extent, the increase of ClONO₂ (not-denitrified vs. denitrified scenario: ~ 0.6 ppb by the end of the time interval) is larger than the decrease of HCl (~ 0.2 ppb), so that in total more ClO_x is converted to reservoir species in the not-denitrified case. Furthermore, the time interval that we investigate is such that in the "with denitrification" case the ozone depletion is still go-

ing on at the end of it, suggesting that the difference between the cases "with denitrification" and "without denitrification" might increase after the time interval we studied. In absence of denitrification the HCl concentration decreases by a factor 2 after PSC evaporation, while the buildup of ClONO₂ even quadrupled, showing how crucially the time taken for chlorine deactivation depends on HNO₃ redistribution due to the gravitational settling of NAT particles.

Summarizing, state-of-the-art microphysical and chemical models are able to simulate the evolution of particles and chemicals in an airmass along a trajectory bordered by two in-situ observations of particles and ozone, and remotely sensed by satellites providing additional informations on key chemical species. The models are effective in explaining the observations, and investigating the relative merit of heterogeneous chemistry on NAT and STS/SSA aerosol and of denitrification on the observed ozone depletion and chlorine partitioning. Under the investigated conditions, NAT PSC presence is of little effectiveness in promoting additional ozone depletion, in comparison with what might be already occurring on background aerosols alone at low temperatures. In our case study, although the influence of denitrification was significant, but of opposite signs, on ClONO₂ and HCl abundances, its impact on ozone depletion was small.

Acknowledgements. The authors acknowledge the Programma Nazionale di Ricerca in Antartide (PNRA) and the Progetto Congiunto di Ricerche CNR-CNRS STRACLIMA for financial support, and the National Science Foundation (NSF) for logistics and technical support on the site. Jennifer Mercer and Terry Deshler were supported by the NSF under, most recently, OPP Grant 0839124. This work was also partially funded by the European Commission under the grant number RECONCILE-226365-FP7-ENV-2008-1.

References

- Achtert, P., Tesche, M.: Assessing lidar-based classification schemes for polar stratospheric clouds based on 16 years of measurements at Esrange, Sweden, *J. Geophys. Res.*, 119(3), 1386-1405, 2014.
- Adriani, A., Deshler, T., Di Donfrancesco, G., Gobbi, G. P.: Polar stratospheric clouds and volcanic aerosol during 1992 spring over McMurdo Station, Antarctica: Lidar and particle counter comparisons, *J. Geophys. Res.*, 100, 25877-25898, 1995.
- Adriani, A., Massoli, P., Di Donfrancesco, G., Cairo, F., Moriconi, M. L., Snels, M.: Climatology of polar stratospheric clouds based on lidar observations from 1993 to 2001 over McMurdo Station, Antarctica, *J. Geophys. Res.*, 109, D24211, doi:10.1029/2004JD004800, 2004.
- Arnone, E., Castelli, E., Papandrea, E., Carlotti, M., Dinelli, B. M.: Extreme ozone depletion in the 2010-2011 Arctic winter stratosphere as observed by MIPAS/ENVISAT using a 2-D tomographic approach, *Atmos. Chem. Phys.*, 12, 9149-9165, 2012.
- Biele, J., Tsias, A., Luo B. P., Carslaw, K. S., Neuber, R., Beyerle, G., Peter, T.: Nonequilibrium coexistence of solid and liquid particles in Arctic stratospheric clouds, *J. Geophys. Res.*, 106(D19), 22991-23007, doi:10.1029/2001JD900188, 2001.
- Brasseur, G.P., Tie, X.X., Rasch, P.J., Lefèvre, F.: A three-dimensional simulation of the Antarctic ozone hole: Impact of anthropogenic chlorine on the lower stratosphere and upper troposphere. *J. Geophys. Res.* 102, 8909-8930, 1997.
- Browell, E. V., Butler, C. F., Ismail, S., Robinette, P. A., Carter, A. F., Higdon, N. S., Toon, O. B., Shoeberl, M. R., Tuck, A. F.: Airborne lidar observations in the wintertime Arctic stratosphere: polar stratospheric clouds, *Geophys. Res. Lett.*, 17, 385-388, 1990.
- Cairo, F., Di Donfrancesco, G., Adriani, A., Pulvirenti, L., Fierli, F.: Comparison of various linear depolarization parameters measured by lidar, *Appl. Opt.*, 38, 4425-4432, 1999.
- Carlotti, M., Brizzi, G., Papandrea, E., Prevedelli, M., Ridolfi, M., Dinelli, B. M., Magnani, L.: GMTR: Two-dimensional geofit multitarget retrieval model for Michelson Interferometer for Passive Atmospheric Sounding/Environmental Satellite observations, *Appl. Opt.*, 45, 716-727, doi:10.1364/AO.45.000716, 2006.
- Carslaw, K.S., Luo, B. P., Peter, T.: An analytic expression for the composition of aqueous HNO₃-H₂SO₄ stratospheric aerosols including gas phase removal of HNO₃, *Geophys. Res. Lett.* 22, 1877-1880, 1995.
- Carslaw, K. S., Peter, T.: Uncertainties in reactive uptake coefficients for solid stratospheric particles - 1. Surface chemistry, *Geophys. Res. Lett.*, 24, 1743-1746, 1997.
- Chayka, A. M., Timofeyev, Y. M., Polyakov, A. V.: Integral Microphysical Parameters of Stratospheric Background Aerosol for 2002-2005 (the SAGE III Satellite Experiment), *Izv. Atmos. Ocean. Phys.*, 44, 206-220, 2008.
- Dee, D. P., Uppala, S. M., Simmons, A. J., Berrisford, P., Poli, P., Kobayashi, S., Andrae, U., Balmaseda, M. A., Balsamo, G., Bauer, P., Bechtold, P., Beljaars, A. C. M., van de Berg, L., Bidlot, J., Bormann, N., Delsol, C., Dragani, R., Fuentes, M., Geer, A. J., Haimberger, L., Healy, S. B., Hersbach, H., Hólm, E. V., Isaksen, I., Kållberg, P., Köhler, M., Matricardi, M., McNally, A. P., Monge-Sanz, B. M., Morcrette, J.-J., Park, B.-K., Peubey, C., de Rosnay, P., Tavolato, C., Thépaut, J.-N., Vitart, F.: The ERA-Interim reanalysis: configuration and performance of the data assimilation system, *Q.J.R. Meteorol. Soc.*, 137, 553-597, doi: 10.1002/qj.828, 2011.
- Deshler, T., Hervig, M. E., Hofmann, D. J., Rosen, J. M., Liley, J. B.: Thirty years of in situ stratospheric aerosol size distribution measurements from Laramie, Wyoming (41° N), using balloon-borne instruments, *J. Geophys. Res.*, 108(D5), 4167, doi:10.1029/2002JD002514, 2003a.
- Deshler, T., Larsen N., Weisser C., Schreiner J., Mauersberger K., Cairo F., Adriani A., Di Donfrancesco G., Ovarlez J., Ovarlez H., Blum U., Fricke K.H., Dörnbrack A., Large nitric acid particles at the top of an Arctic stratospheric cloud, *J. Geophys. Res.*, 108(D16), 4517, doi:10.1029/2003JD003479, 2003b.
- Deshler, T., Mercer J. M., Smit H. G. J., Stubi R., Levrat G., Johnson B. J., Oltmans S. J., Kivi R., Thompson A. M., Witte J., Davies J., Schmidlin F. J., Brothers G., Sasaki T.: Atmospheric comparison of electrochemical cell ozonesondes from different manufacturers, and with different cathode solution strengths: The Balloon Experiment on Standards for Ozonesondes, *J. Geophys. Res.*, 113, D04307, doi:10.1029/2007JD008975, 2008.

- Di Liberto, L., Cairo, F., Fierli, F., DiDonfrancesco, G., Viterbini, M., Deshler, T., Snelms, M.: Observation of Polar Stratospheric clouds over McMurdo (77.85 S, 166.67 E) (2006-2010), *J. Geophys. Res. Atmos.*, 119, doi:10.1122/2013JD019892, 2014.
- 905 Dinelli, B. M., Arnone, E., Brizzi, G., Carlotti, M., Castelli, E., Magnani, L., Papandrea, E., Prevedelli, M., Ridolfi, M.: The MIPAS2D database of MIPAS/ENVISAT measurements retrieved with a multi-target 2-dimensional tomographic approach, *Atmos. Meas. Tech.*, 3, 355-374, 2010.
- 910 Douglass, A. R., Schoeberl, M. R., Stolarski, R. S., Waters, J. W., Russell, J. M., Roche, A. E., Massie, S. T.: Interhemispheric differences in springtime production of HCl and ClONO₂ in the polar vortices, *J. Geophys. Res.*, 100(D7), 13967-13978, 1995.
- 915 Drdla, K., Müller R.: Temperature thresholds for chlorine activation and ozone loss in the polar stratosphere, *Ann. Geophys.*, 30, 1055-1073, 2012.
- Dye, J. E., Baumgardner, D., Gandrud, B. W., Kawa, S. R., Kelly, K. K., Loewenstein, M., Ferry, G. V., Chan, K. R., Gary, B. L.: Particle Size Distributions in Arctic Polar Stratospheric Clouds, Growth and Freezing of Sulfuric Acid Droplets, and Implications for Cloud Formation, *J. Geophys. Res.*, 97, 8015-8034, doi:10.1029/91JD02740, 1992.
- 920 Engel, I., Luo, B. P., Pitts M. C., Poole, L. R., Hoyle, C. R., Grooß, J.-U., Dörnbrack, A., Peter, T.: Heterogeneous Formation of Polar Stratospheric Clouds - Part 2: Nucleation of Ice on Synoptic Scales, *Atmos. Chem. Phys.*, 13, 10769-10785, 2013.
- 925 Engel, I., Luo, B. P., Khaykin, S. M., Wienhold, F. G., Vömel, H., Kivi, R., Hoyle, C. R., Grooß, J.-U., Pitts, M. C., Peter, T.: Arctic stratospheric dehydration - Part 2: Microphysical modeling, *Atmos. Chem. Phys.*, 14, 3231-3246, 2014.
- 930 Fischer, H., Birk, M., Blom, C., Carli, B., Carlotti, M., von Clarman, T., Delbouille, L., Dudhia, A., Ehalt, D., Endemann, M., Flaud, J. M., Gessner, R., Kleinert, A., Koopman, R., Langen, J., Lopez-Puertas, M., Mosner, P., Nett, H., Oelhaf, H., Perron, G., Remedios, J., Ridolfi, M., Stiller, G., Zander, R.: MIPAS: an instrument for atmospheric and climate research, *Atmos. Chem. Phys.*, 8, 2151-2188, 2008.
- 935 Froidevaux, L., Livesey, N. J., Read, W. G., Jiang, Y. B., Jimenez, C., Filipiak, M. J., Schwartz, M. J., Santee, M. L., Pumphrey, H. C., Jiang, J. H., Wu, D. L., Manney, G. L., Drouin, B. J., Waters, J. W., Fetzer, E. J., Bernath, P. F., Boone, C. D., Walker, K. A., Jucks, K. W., Toon, G. C., Margitan, J. J., Sen, B., Webster, C. R., Christensen, L. E., Elkins, J. W., Atlas, E., Lueb, R. A., Hendershot, R.: Early Validation Analyses of Atmospheric Profiles From EOS MLS on the Aura Satellite, *IEEE Trans. Geosci. Remote Sensing*, 44, 1106-1121, 2006.
- 940 Gobbi, G. P.: Lidar estimation of stratospheric aerosol properties: Surface, volume, and extinction to backscatter ratio, *J. Geophys. Res.*, 100(D6), 11219-11235, 1995.
- 945 Grooß, J. U., Pierce, R. B., Crutzen, P. J., Grose, W. L., Russell, J. M.: Re-formation of chlorine reservoirs in southern hemisphere polar spring, *J. Geophys. Res.*, 102(D11), 13141-13152, 1997.
- 950 Grooß, J. U., Brauttsch, K., Pommerich, R., Solomon, S., Müller, R.: Stratospheric ozone chemistry in the Antarctic: what determines the lowest ozone values reached and their recovery?, *Atmos. Chem. Phys.*, 11, 12217-12226, 2011.
- Hitchman, M. H., McKay, M. Trepte, C. R.: A climatology of stratospheric aerosol, *J. Geophys. Res.*, 99(D10), 20689-20700, 1994.
- Hofmann, D. J., Deshler, T.: Stratospheric cloud observations during formation of the Antarctic ozone hole in 1989, *J. Geophys. Res.*, 96(D2), 2897-2912, 1991.
- Hoppel, K., Bevilacqua, R., Canty, T., Salawitch, R., Santee, M.: A measurement/model comparison of ozone photochemical loss in the Antarctic ozone hole using Polar Ozone and Aerosol Measurement observations and the Match technique, *J. Geophys. Res.*, 110, D19304, doi:10.1029/2004JD005651, 2005.
- Hoyle, C. R., Engel, I., Luo, B. P., Pitts, M. C., Poole, L. R., Grooß, J.-U., Peter, T.: Heterogeneous Formation of Polar Stratospheric Clouds - Part 1: Nucleation of Nitric Acid Trihydrate (NAT), *Atmos. Chem. Phys.*, 13, 9577-9595, 2013.
- Komhyr, W. D.: Electrochemical concentration cells for gas analysis, *Ann. Geophys.*, 25, 203-210, 1969.
- Konopka, P., Steinhorst, H. M., Grooß, J. U., Günther, G., Müller, R., Elkins, J. W., Jost, H.J., Richard, E., Schmidt, U., Toon, G., McKenna, D. S.: Mixing and ozone loss in the 1999-2000 Arctic vortex: Simulations with the three-dimensional Chemical Lagrangian Model of the Stratosphere (CLaMS), *J. Geophys. Res.*, 109(D2), D02315, doi:10.1029/2003JD003792, 2004.
- Koop, T., Luo, B. P., Tsias, A., Peter, T.: Water activity as the determinant for homogeneous ice nucleation in aqueous solutions, *Nature*, 406, 611-614, doi:10.1038/35020537, 2000.
- Kröger, C., Hervig, M., Nardi, B., Oolman, L., Deshler, T., Wood, S., Nichol, S.: Stratospheric ozone reaches new minima above McMurdo Station, Antarctica, between 1998 and 2001, *J. Geophys. Res.*, 108(D17), 4555-4567, doi:10.1029/2002JD002904, 2003.
- Lambert, A., Santee, M. L., Wu, D. L., Chae, J. H.: A-train CALIOP and MLS observations of early winter Antarctic polar stratospheric clouds and nitric acid in 2008, *Atmos. Chem. Phys.*, 12, 2899-2931, doi:10.5194/acp-12-2899-2012, 2012.
- Lowe, D., MacKenzie, A. R.: Polar stratospheric cloud microphysics and chemistry, *J. Atmos. Sol.-Terr. Phys.*, 70, 13-40, 2008.
- Nardi, B., Bellon, W., Oolman, L. D., Deshler, T.: Spring 1996 and 1997 ozonesonde measurements over McMurdo Station, Antarctica, *Geophys. Res. Lett.*, 723-726, 1999.
- Luo, B. P., Voigt, C., Fueglistaler, S., Peter, T.: Extreme NAT supersaturations in mountain wave ice PSCs: A clue to NAT formation, *J. Geophys. Res.*, 108, 4441, doi:10.1029/2002JD003104, 2003.
- Maturilli, M., Neuber, R., Massoli, P., Cairo, F., Adriani, A., Moriconi, M. L., Di Donfrancesco G.: Differences in Arctic and Antarctic PSC occurrences observed by lidar in Ny-MAlesund (79 N, 12 E) and McMurdo (78 S, 167 E), *Atmos. Chem. Phys.*, 5, 2081-2090, 2005.
- McKenna, D. S., Konopka, P., Grooß, J.-U., Günther, G., Müller, R., Spang, R., Offerman, D., Orsolini, Y.: A new Chemical Lagrangian Model of the Stratosphere (CLaMS): 1. Formulation of advection and mixing, *J. Geophys. Res.*, 107(D16), doi:10.1029/2000JD000114, 2002a.
- McKenna, D. S., Grooß, J.-U., Günther, G., Konopka, P., Müller, R., Carver, G., Sasano, Y.: A new Chemical Lagrangian Model of the Stratosphere (CLaMS): 2. Formulation of chemistry scheme and initialization, *J. Geophys. Res.*, 107(D15), doi:10.1029/2000JD000113, 2002b.
- Mercer, J. L., Kröger, C., Nardi, B., Johnson, B. J., Chipperfield, M. P., Wood, S. W., Nichol, S. E., Santee, M. L., Deshler, T.: Comparison of measured and modeled ozone above McMurdo

- Station, Antarctica, 1989-2003, during austral winter/spring, *J. Geophys. Res.*, 112, D19307, doi:10.1029/2006JD007982, 2007.
- Mishchenko, M. I., Travis, L. D., Mackowski, D. W.: T-Matrix Computations of Light Scattering by Nonspherical Particles: A Review, *J. Quant. Spectrosc. Radiat. Transf.*, 111, 1704-1744, doi:10.1016/0022-4073(96)00002-7, 2010.
- Molleker, S., Borrmann, S., Schlager, H., Luo, B. P., Frey, W., Klingebiel, M., Weigel, R., Ebert, M., Mitev, V., Matthey, R., Woiwode W., H. Oelhaf, Dörnbrack A., G. Stratmann, Groß, J-U., Günther G., Vogel B., Müller R., Krämer M., Meyer J., F. Cairo: Microphysical properties of synoptic scale polar stratospheric clouds: In-situ measurements of unexpectedly large HNO₃ containing particles in the Arctic vortex, *Atmos. Chem. Phys.*, 14, 10785-10801, 2014.
- Nardi, B., Bellon, W., Oolman, L. D., Deshler, T.: Spring 1996 and 1997 ozonesonde measurements over McMurdo Station, Antarctica, *Geophys. Res. Lett.*, 26, 723-726, 1999.
- Pitts, M. C., Thomason, L. W., Poole, L. R., Winker, D. M.: Characterization of polar stratospheric clouds with spaceborne lidar: CALIPSO and the 2006 Antarctic season, *Atmos. Chem. Phys.*, 7, 5207-5228, doi:10.5194/acp-7-5207-2007, 2007.
- Pitts, M. C., Poole, L. R., and Thomason, L. W.: CALIPSO polar stratospheric cloud observations: second-generation detection algorithm and composition discrimination, *Atmos. Chem. Phys.*, 9, 7577-7589, doi:10.5194/acp-9-7577-2009, 2009.
- Pitts, M. C., Poole, L. R., Dörnbrack, A., Thomason, L. W.: The 2009-2010 Arctic polar stratospheric cloud season: a CALIPSO perspective, *Atmos. Chem. Phys.*, 11, 2161-2177, doi:10.5194/acp-11-2161-2011, 2011.
- Plöger F., Konopka P., Günther G., Groß J.-U., Müller R.: Impact of the vertical velocity scheme on modeling transport in the tropical tropopause layer, *J. Geophys. Res.*, 115, D03301, doi:10.1029/2009JD012023, 2010.
- Raspollini, P., Carli, B., Carlotti, M., Ceccherini, S., Dehn, A., Dinelli, B. M., Dudhia, A., Flaud, J-M., L-Puertas, M., Niro, F., Remedios, J. J., Ridolfi, M., Sembhi, H., Sgheri, L., von Clarermann, T.: Ten years of MIPAS measurements with ESA Level 2 processor V6 - Part 1: Retrieval algorithm and diagnostics of the products, *Atmos. Meas. Tech.*, 6, 2419-2439, doi:10.5194/amt-6-2419-2013, 2013.
- Riviere, E. D.: A Lagrangian method to study stratospheric nitric acid variations in the polar regions as measured by the Improved Limb Atmospheric Spectrometer, *J. Geophys. Res.*, 108, D23, doi:10.1029/2003JD003718, 2003.
- Russell, P. B., Swissler, T. J., McCormick, M. P.: Methodology for error analysis and simulation of lidar aerosol measurements, *Appl. Optics*, 18, 3783-3797, 1979.
- Sander, S.P.S, Friedl, R. R., Barker, J. R., Golden, D. M., Kurylo, M. J., Wine, P. H., Abbatt, J. P. D., Burkholder, J. B., Kolb, C. E., Moortgat, G. K., Huie, R. E., Orkin, V. L.: Chemical Kinetics and Photochemical Data for Use in Atmospheric Studies, Evaluation Number 17. JPL Publication 10-06, Jet Propulsion Laboratory, Pasadena, California, 2011.
- Santee, M. L., Tabazadeh A., Manney G. L., Fromm M. D., Bevilacqua R. M., Waters J. W., Jensen E. J.: A Lagrangian approach to studying Arctic polar stratospheric clouds using UARS MLS HNO₃ and POAM II aerosol extinction measurements, *J. Geophys. Res.*, 107(D10), doi:10.1029/2000JD000227, 2002.
- Santee, M. L., Lambert, A., Read, W. G., Livesey, N. J., Cofield, R. E., Cuddy, D. T., Daffer W. H., Drouin, B. J., Froidevaux, L., Fuller, R. A., Jarnot, R. F., Knosp, B. W., Manney, G. L., Perun, V. S., Snyder, W. V., Stek, P. C., Thurstans, R. P., Wagner, P. A., Waters, J. W., Muscari, G., de Zafra, R. L., Dibb, J. E., Fahey, D. W., Popp, P. J., Marcy, T. P., Jucks, K. W., Toon, G. C., Stachnik, R. A., Bernath, P. F., Boone, C. D., Walker, K. A., Urban, J., Murtagh, D.: Validation of the Aura Microwave Limb Sounder HNO₃ Measurements, *J. Geophys. Res.*, 112, D24S40, doi:10.1029/2007JD008721, 2007.
- Sasano, Y., Terao, Y., Tanaka, H. L., Yasunari, T., Kanzawa, H., Nakajima, H., Yokota, T., Nakane, H., Hayashida, S., Saitoh, N.: ILAS observations of chemical ozone loss in the Arctic vortex during early spring 1997, *Geophys. Res. Lett.*, 27(2), 213 - 216, 2000.
- Schofield, R., Avallone, L. M., Kalnajs, L. E., Hertzog, A., Wohltmann, I., and Rex, M.: First quasi-Lagrangian in situ measurements of Antarctic Polar springtime ozone: observed ozone loss rates from the Concordiasi long-duration balloon campaign, *Atmos. Chem. Phys.*, 15, 2463-2472, doi:10.5194/acp-15-2463-2015, 2015.
- Snels, M., Cairo, F., Colao, F., Di Donfrancesco, G.: Calibration method for depolarization lidar measurements, *Int. J. Remote Sens.*, 30, 5725-5736, doi:10.1080/01431160902729572, 2009.
- Solomon, S., Garcia, R. R., Rowland, F. S., Wuebbles, D. J.: On the depletion of Antarctic ozone, *Nature*, 321, 755-758, 1986.
- Solomon, S.: Stratospheric ozone depletion: A review of concepts and history, *Rev. Geophys.*, 37, 275-316, 1999.
- Steinbrecht, W., Claude, H., Schönenborn, F., Leiterer, U., Dier, H., Lanzinger, E.: Pressure and Temperature Differences between Vaisala RS80 and RS92 Radiosonde-Systems, *J. Atmos. Ocean. Tech.*, 25, 909-927, doi:10.1175/2007JTECHA999.1, 2008.
- Stephens, G.L., Vane, D.G., Boain, R.J., Mace, G.G., Sassen, K., Wang, Z., Illingworth, A.J., O'Connor, E.J., Rossow, W.B., Durdin, S.L., Miller, S.D., Austin, R.T., Benedetti, A., Mitrescu, C., and CloudSat Science Team: The CloudSat mission and the A-Train: A new dimension of space-based observations of clouds and precipitation, *Bull. Amer. Meteorol. Soc.*, 83, 1771-1790, doi:10.1175/BAMS-83-12-1771, 2002.
- Terao, Y., Sasano, Y., Nakajima, H., Tanaka, H. L., Yasunari, T.: Stratospheric ozone loss in the 1996/1997 Arctic winter: Evaluation based on multiple trajectory analysis for double-sounded air parcels by ILAS, *J. Geophys. Res.*, 107(D24), 8210, doi:10.1029/2001JD000615, 2002.
- Toon, O. B., Browell, E. V., Kinne, S., Jordan, J.: An analysis of lidar observations of polar stratospheric clouds, *Geophys. Res. Lett.*, 17, 393-396, 1990.
- Tsias, A., Wirth, M., Carslaw, K. S., Biele, J., Mehrtens, H., Reichardt, J., Wedekind C., Weiß, V., Renger W., Neuber R., von Zahn U., Stein B., Santacesaria V., Stefanutti L., Fierli F., Bacmeister J., Peter T.: Aircraft lidar observations of an enhanced type Ia polar stratospheric clouds during APE-POLECAT, *J. Geophys. Res.*, 104(D19), 23961-23969, 1999.
- Voigt, C., Schreiner, J., Kohlmann, A., Zink, P., Mauersberger, K., Larsen, N., Deshler, T., Kröger C., Rosen, J., Adriani, A., Cairo, F., Di Donfrancesco, G., Viterbini, M., Ovarlez, J., Ovarlez, H., David, C., Dörnbrack A.: Nitric Acid Trihydrate (NAT) in Polar Stratospheric Clouds, *Science*, 290, 1756-1758, 2000.

- von Hobe, M., Bekki, S., Borrmann, S., Cairo, F., D'Amato, F.,
Di Donfrancesco, G., Dörnbrack, A., Ebersoldt, A., Ebert, M.,
1135 Emde, C., Engel, I., Ern, M., Frey, W., Genco, S., Griessbach,
S., Groß, J.-U., Gulde, T., Günther, G., Hösen, E., Hoffmann,
L., Homonnai, V., Hoyle, C. R., Isaksen, I. S. A., Jackson, D. R.,
Jánosi, I. M., Jones, R. L., Kandler, K., Kalicinsky, C., Keil, A.,
Khaykin, S. M., Khosrawi, F., Kivi, R., Kuttippurath, J., Laube,
1140 J. C., Lefe, F., Lehmann, R., Ludmann, S., Luo, B. P., Marc-
hand, M., Meyer, J., Mitev, V., Molleker, S., Müller, R., Oelhaf,
H., Olschewski, F., Orsolini, Y., Peter, T., Pfeilsticker, K., Piesch,
C., Pitts, M. C., Poole, L. R., Pope, F. D., Ravegnani, F., Rex,
M., Riese, M., Röckmann, T., Rognerud, B., Roiger, A., Rolf,
1145 C., Santee, M. L., Scheibe, M., Schiller, C., Schlager, H., Sicil-
iani de Cumis, M., Sitnikov, N., Svde, O. A., Spang, R., Spelten,
N., Stordal, F., Sumińska-Ebersoldt, O., Ulanovski, A., Unger-
mann, J., Viciani, S., Volk, C. M., vom Scheidt, M., von der Ga-
then, P., Walker, K., Wegner, T., Weigel, R., Weinbruch, S., Wet-
1150 zel, G., Wienhold, F. G., Wohltmann, I., Woiwode, W., Young,
I. A. K., Yushkov, V., Zobrist, B., and Strohm, F.: Reconciliation
of essential process parameters for an enhanced predictability of
Arctic stratospheric ozone loss and its climate interactions (REC-
ONCILE): activities and results, *Atmos. Chem. Phys.*, 13, 9233-
1155 9268, doi:10.5194/acp-13-9233-2013, 2013.
- Waters, J. W., Froidevaux, L., Harwood, R. S., Jarnot, R. F., Pickett,
H. M., Read, W. G., Siegel, P. H., Cofield, R. E., Filipiak, M. J.,
Flower, D. A., Holden, J. R., Lau, G. K., Livesey, N. J., Man-
ney, G. L., Pumphrey, H. C., Santee, M. L., Wu, D. L., Cuddy, D.
1160 T., Lay, R. R., Loo, M. S., Perun, V. S., Schwartz, M. J., Stek,
P. C., Thurstans, R. P., Boyles, M. A., Chandra, K. M., Chavez,
M. C., Chen, G.-S., Chudasama, B. V., Dodge, R., Fuller, R. A.,
Girard, M. A., Jiang, J. H., Jiang, Y., Knosp, B. W., LaBelle, R.
C., Lam, J. C., Lee, K. A., Miller, D., Oswald, J. E., Patel, N.
1165 C., Pukala, D. M., Quintero, O., Scaff, D. M., Van Snyder, W.,
Tope, M. C., Wagner, P. A., Walch, M. J.: The Earth Observ-
ing System Microwave Limb Sounder (EOS MLS) on the Aura
Satellite, *IEEE Trans. Geosci. Remote Sens.*, 441075-1092, doi
10.1109/TGRS.2006.873771, 2006.
- 1170 Wegner, T., Groß, J.-U., von Hobe, M., Strohm, F., Sumińska-
Ebersoldt, O., Volk, C. M., Hösen, E., Mitev, V., Shur, G., Müller,
R.: Heterogeneous chlorine activation on stratospheric aerosols
and clouds in the Arctic polar vortex, *Atmos. Chem. Phys.*, 12,
11095-11106, doi:10.5194/acp-12-11095-2012, 2012.
- 1175 Wohltmann, I., Wegner, T., Müller, R., Lehmann, R., Rex, M., Man-
ney, G. L., Santee, M. L., Bernath, P., Sumińska-Ebersoldt, O., Strohm,
F., von Hobe, M., Volk, C. M., Hösen, E., Ravegnani, F., Ulanovsky
A., Yushkov, V.: Uncertainties in modelling heterogeneous chem-
1180 istry and Arctic ozone depletion in the winter 2009/2010. *Atmos.
Chem. Phys.* 13, 3909-3929, 2013.

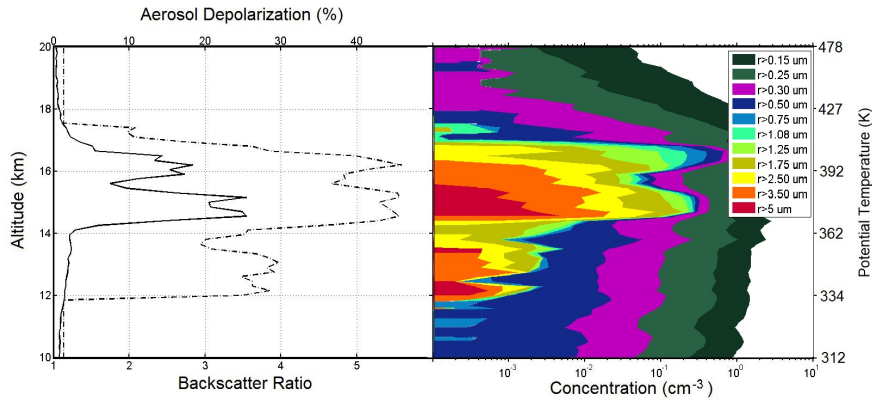


Figure 1. Left panel, altitude profiles of Backscatter (solid line) and Aerosol Depolarization (dashed line) Ratio measured by lidar. Right panel, altitude profiles of Optical Particle Counter integrated size distributions, the colors indicate different lower diameter thresholds from $0.15 \mu\text{m}$ to $5 \mu\text{m}$, as reported in the legend.

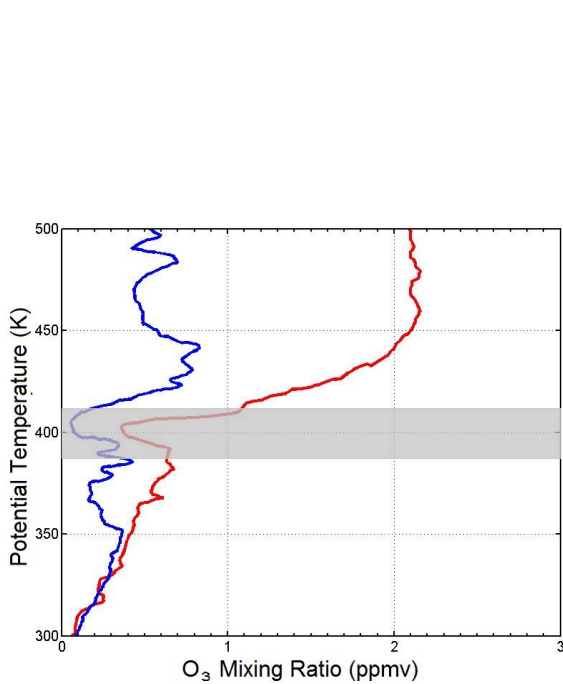


Figure 2. O_3 measurements from the in-situ ozonesonde (red line) on 10 Sept 2008, and on 20 Sept 2008 (blue line), vs potential temperature. The grey area highlights the air layer which returned over the Ross Sea less than 300 km from McMurdo.

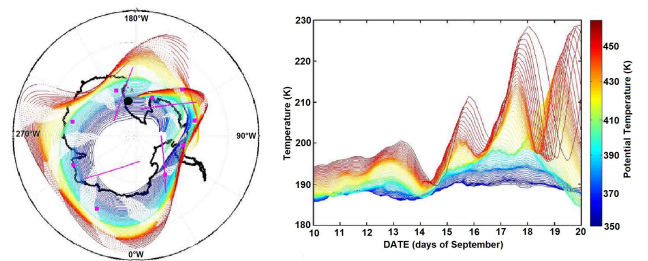


Figure 3. Left panel, air mass trajectories originating from McMurdo (black dot) and run 10 days forward, colour coded according to potential temperature. Solid coloured lines indicate sunlit legs, dotted lines indicate legs in darkness. Purple lines specify intersections with CALIOP footprint. Purple dots indicate where MLS data (O_3 , HNO_3 or HCl) were available. Right panel, temperature values along the trajectories, again colour coded in term of potential temperature.

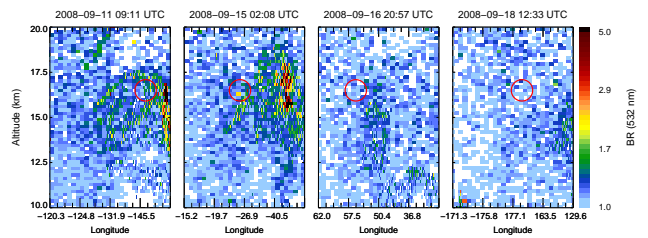


Figure 4. CALIOP Backscatter Ratio (colour coded) vs altitude and longitude. Red circles highlight the intersection with the 400K isentropic trajectory.

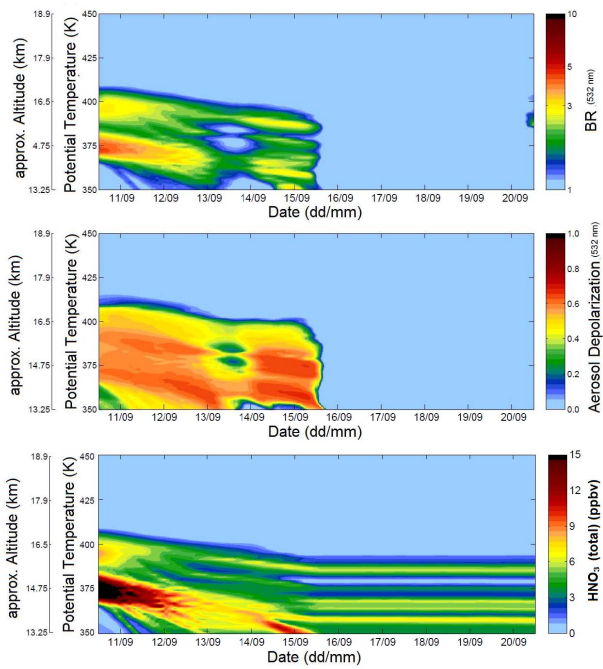


Figure 5. Profiles of Backscatter Ratio (upper panel), Aerosol Depolarization Ratio (middle panel) and total HNO_3 (lower panel) starting from the observations taken on September 10, 2008, and evolving according to the microphysical model.

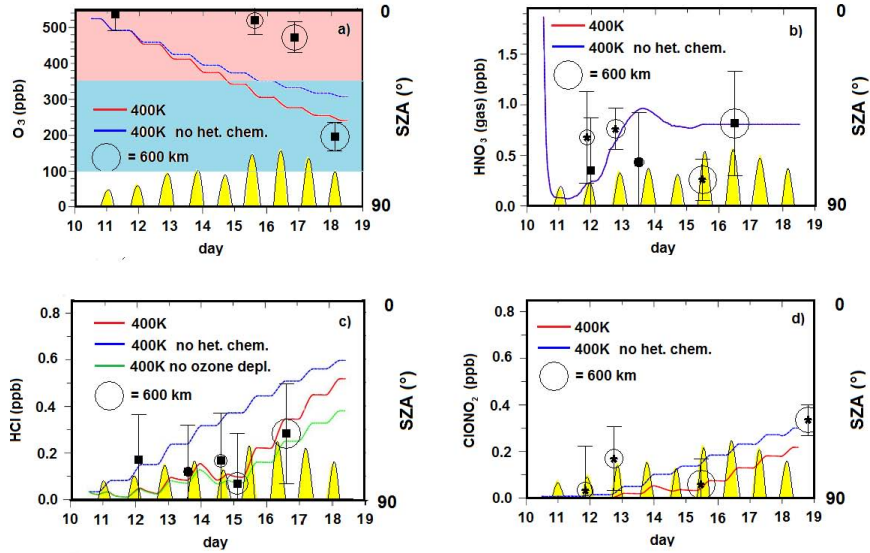


Figure 6. MLS (squares) and MIPAS (stars) observations and model results with (red line) and without (blue line) heterogeneous chemistry. a) (upper left panel) O_3 the colored areas highlight the range of variability of O_3 values observed by the balloonborne ozone sonde in the 400 ± 10 K air layer which returned over the Ross Sea less than 300 km from McMurdo: Red for the first flight, Blue for the second flight ; b) (upper right) HNO_3 ; c) (lower left) HCl ; d) (lower right) $ClONO_2$. The radius of the circles surrounding the data points represents the match radius. Yellow areas indicate sunlit parts of the trajectory, the corresponding solar zenith angle (SZA) is reported on the right vertical axis.

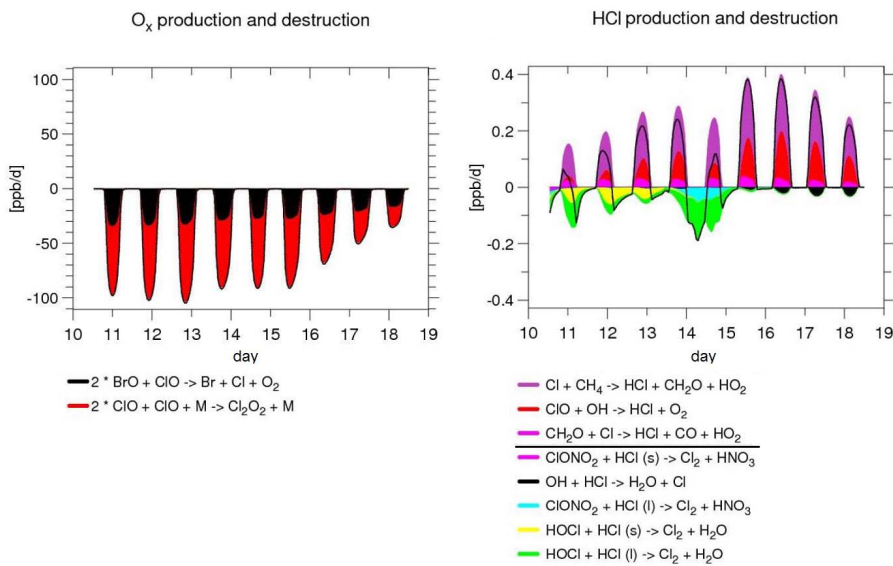


Figure 7. Left panel: O_3 depletion rates due to ClO - BrO (black) and ClO - ClO (red) catalytic cycles. Right panel: HCl production and depletion rates due to the set of reactions listed at the bottom of the panel. Simulation have been carried out on the 400 K isentropic level.

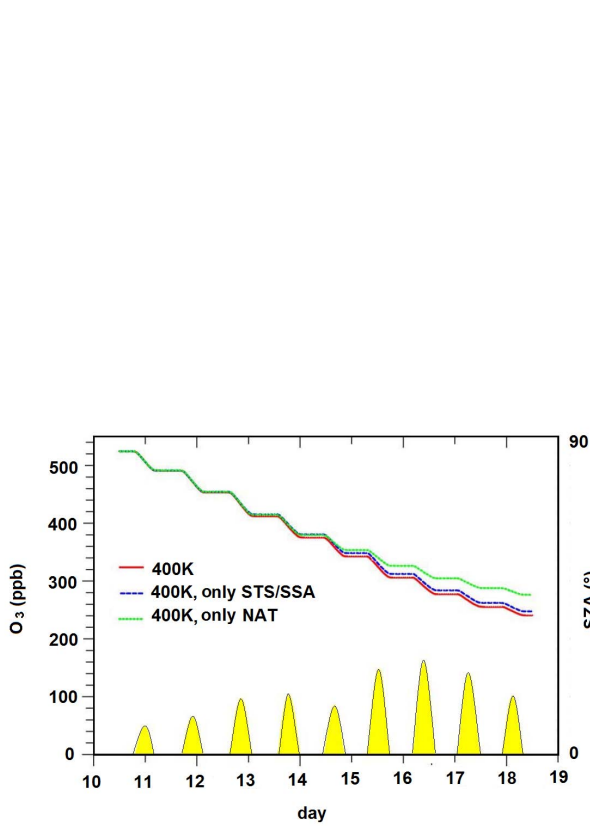


Figure 8. O_3 evolution taking into account the full heterogeneous chemistry (red), or going on only on NAT (green) or on STS/SSA (blue).

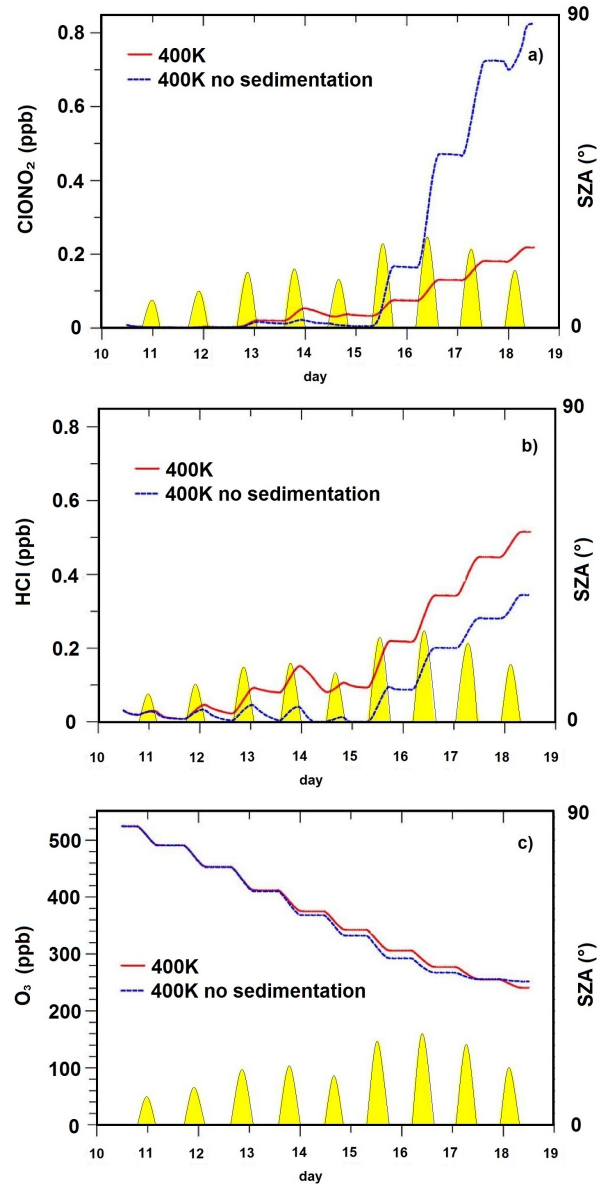


Figure 9. $ClONO_2$ (upper panel), HCl (middle) and O_3 (lower) evolution with (red line) and without (blue line) denitrification due to particle sedimentation.